Atmos. Chem. Phys., 9, 7623–7641, 2009
www.atmos-chem-phys.net/9/7623/2009/

Atmospheric Chemistry and Physics

Closing the peroxy acetyl nitrate budget: observations of acyl peroxy nitrates (PAN, PPN, and MPAN) during BEARPEX 2007

B. W. LaFranchi[1], G. M. Wolfe[2], J. A. Thornton[3], S. A. Harrold[3], E. C. Browne[1], K. E. Min[4], P. J. Wooldridge[1], J. B. Gilman[5], W. C. Kuster[5], P. D. Goldan[5], J. A. de Gouw[5], M. McKay[6,*], A. H. Goldstein[6], X. Ren[7,], J. Mao[7,***], and R. C. Cohen[1,4]**

[1]Department of Chemistry, University of California, Berkeley, Berkeley, CA, USA
[2]Department of Chemistry, University of Washington, Seattle, WA, USA
[3]Department of Atmospheric Sciences, University of Washington, Seattle, WA, USA
[4]Department of Earth and Planetary Science, University of California, Berkeley, CA, USA
[5]NOAA/ESRL Chemical Sciences Division, Boulder, CO, USA
[6]Department of Environmental Science, Policy, and Management, University of California, Berkeley, Berkeley, CA, USA
[7]Department of Meteorology, Penn State University, University Park, PA, USA
[*]now at: California Air Resources Board, Sacramento, CA, USA
[**]now at: Rubenstein School of Marine and Atmospheric Science, University of Miami, Miami, FL, USA
[***]now at: School of Engineering and Applied Sciences, Harvard University, Cambridge, MA, USA

Received: 1 April 2009 – Published in Atmos. Chem. Phys. Discuss.: 20 April 2009
Revised: 2 September 2009 – Accepted: 3 September 2009 – Published: 12 October 2009

Abstract. Acyl peroxy nitrates (APNs, also known as PANs) are formed from the oxidation of aldehydes and other oxygenated VOC (oVOC) in the presence of NO_2. There are both anthropogenic and biogenic oVOC precursors to APNs, but a detailed evaluation of this chemistry against observations has proven elusive. Here we describe measurements of PAN, PPN, and MPAN along with the majority of chemicals that participate in their production and loss, including OH, HO_2, numerous oVOC, and NO_2. Observations were made during the Biosphere Effects on AeRosols and Photochemistry Experiment (BEARPEX 2007) in the outflow of the Sacramento urban plume. These observations are used to evaluate a detailed chemical model of APN ratios and concentrations. We find that the ratios of APNs are nearly independent of the loss mechanisms and thus an especially good test of our understanding of their sources. We show that oxidation of methylvinyl ketone, methacrolein, methyl glyoxal, biacetyl and acetaldehyde are all significant sources of the PAN+peroxy acetyl (PA) radical reservoir, accounting for 26%, 2%, 7%, 20%, and 45%, of the production rate on average during the campaign, respectively. At high temperatures, when upwind isoprene emissions are highest, oxidation of non-acetaldehyde PA radical sources contributes over 60% to the total PA production rate, with methylvinyl ketone being the most important of the isoprene-derived sources. An analysis of absolute APN concentrations reveals a missing APN sink that can be resolved by increasing the PA+ΣRO_2 rate constant by a factor of 3.

Correspondence to: J. A. Thornton
(thornton@atmos.washington.edu)

1 Introduction

Acyl peroxy nitrates (APNs, also known as PANs) are an important class of reactive nitrogen species having the general structure: $RC(O)OONO_2$. In urban source regions, APN production acts as a net sink for NO_x (NO_x=NO+NO_2). Under high NO_x (VOC-limited) conditions this temporary sink results in increased ozone production rates by slowing the rate of OH reaction with NO_2, and thus extending the HO_x (HO_x=OH+HO_2) chain length. Downwind of the source region, where total NO_x levels have decreased, APN decomposition injects NO_x into the atmosphere under low NO_x conditions resulting in increased ozone production rates. This latter effect has been discussed extensively with respect to

production of ozone in the remote troposphere (Moxim et al., 1996; Kotchenruther et al., 2001; Hudman et al., 2004; Parrish et al., 2004), but it is also relevant to regions immediately outside of urban areas (Sillman and Samson, 1995; Olszyna et al., 1997; Lei et al., 2007).

APN formation is initiated by the reaction of the hydroxyl radical (OH) with or by photolysis of aldehydes, ketones, and other oxygenated volatile organic compounds (oVOCs) (Reaction R1a and R1b). When the product of these reactions is an acyl peroxy (AP) radical with the general structure, $RC(O)O_2$, then reversible reactions with NO_2 to form APNs can occur (Reaction R2a and R2b).

$$\text{oVOC}+\text{OH}(+\text{O}_2)\longrightarrow \text{RC(O)O}_2 \quad \text{(R1a)}$$

$$\text{oVOC}+h\nu(+\text{O}_2)\longrightarrow \text{RC(O)O}_2 \quad \text{(R1b)}$$

$$\text{RC(O)O}_2+\text{NO}_2\longrightarrow \text{RC(O)OONO}_2 \quad \text{(R2a)}$$

$$\text{RC(O)OONO}_2\longrightarrow \text{RC(O)O}_2+\text{NO}_2 \quad \text{(R2b)}$$

$$\text{RC(O)O}_2+\text{NO}\longrightarrow \text{products} \quad \text{(R3)}$$

$$\text{RC(O)O}_2+\text{HO}_2\longrightarrow \text{products} \quad \text{(R4)}$$

$$\text{RC(O)O}_2+\text{RO}_2\longrightarrow \text{products} \quad \text{(R5)}$$

$$\text{RC(O)OONO}_2+\text{OH}\longrightarrow \text{products} \quad \text{(R6)}$$

There is a strong temperature dependence to the equilibrium between APNs and their AP radical intermediates ($RC(O)O_2$), and to the APN lifetime with respect to thermal decomposition. At high temperatures, the rapid equilibrium (Reaction R2) makes it useful to combine APNs and their corresponding AP radicals into a chemical family, denoted as APN_T, as shown in Scheme 1a. In this situation, loss of APN_T, and therefore APNs, is limited by reaction of the AP radical with NO (Reaction R3), HO_2 (Reaction R4), or RO_2 (Reaction R5). At low temperatures, equilibration within the APN_T reservoir is slower. In this situation, described by Scheme 1b, loss of APN_T is limited by the thermal decomposition rate of the APN and, in some cases, reaction of the APN with OH.

In addition to gas phase chemical removal, the APN_T reservoir can be removed from the atmosphere by reactions in aerosol and fog (Roberts et al., 1996) or by dry deposition (Turnipseed et al., 2006; Farmer and Cohen, 2008; Wolfe et al., 2009). APN_T deposition can be an effective net sink for NO_x if APNs are lost to surfaces, or it can serve as a source of NO_x if deposition of the corresponding AP radical and concurrent release of NO_x is important. APN deposition has been discussed as a potentially important source of nitrogen to plants (Sparks et al., 2003; Wolfe et al., 2009), with implications for ecosystem productivity (Magnani et al., 2007), soil acidification, and nitrate concentrations in run-off (Bytnerowicz and Fenn, 1996; Goulding et al., 1998).

Many APNs are associated with a single oVOC precursor. For example, peroxy propionyl nitrate (PPN) is believed to be exclusively derived from propanal and methacryloyl peroxy nitrate (MPAN) exclusively from methacrolein (Williams et al., 1997; Roberts et al., 2001). However, PAN, which typically comprises about 80% of the total speciated APNs (Roberts et al., 2007), has multiple oVOC sources. Detailed chemical mechanisms indicate that in addition to acetaldehyde, the isoprene oxidation products methyl glyoxal (MGLY), methylvinyl ketone (MVK), and methacrolein (MACR) are also potential sources of the peroxy acetyl (PA) radical, the precursor to PAN. Consistent with this expectation, Roberts et al. (2001, 2002) found that for Nashville, TN, a region heavily impacted by isoprene emissions, production of PA radicals was significantly higher than could be accounted for by acetaldehyde alone. Observations of PAN off the coast of New England (Roberts et al., 2006) similarly showed a missing PA radical source that correlated with isoprene influence. A study using measurements of total peroxy nitrates (ΣPNs) and the individual precursor aldehydes at another isoprene-impacted site, immediately downwind of Sacramento, CA, led Cleary et al. (2007) to conclude that a PA radical source 3 times greater than that from acetaldehyde was necessary to bring their estimate of PAN/ΣPNs close to the $\sim$80% levels consistently reported elsewhere. Conversely, in Houston, TX, a heavily urbanized area with limited isoprene influence, PAN concentrations were consistent with an acetaldehyde source without the need for other oVOC (Roberts et al., 2001). Global modeling studies (Horowitz et al., 1998; Folberth et al., 2006) using explicit isoprene chemistry reach the same conclusion as the observational studies–that isoprene emissions are a significant driver of PAN production.

A different approach was taken by Grosjean et al. (2002), who used observations of VOCs from Porto Alegre, Brazil as inputs into the SAPRC 97 model and determined that a lumped class of reactive aromatic compounds was a significant contributor to a series of dicarbonyls, including methyl glyoxal, which will lead to PAN formation. No comparison of the model PAN output to observations was made in this study, nor has there been any other study, to date, that has verified the mechanisms of PA radical production by directly comparing PAN measurements to calculations based on the observed oVOC source distribution. With this in mind, the primary objective of this study is to evaluate a comprehensive chemical mechanism for production of the PA radical by comparison to observations. We approach this objective by making use of a steady-state model to determine whether mixing ratios of PAN, MPAN, and PPN, are in balance with their known sources and sinks. Cleary et al. (2007) evaluated a steady model of APNs against a time-dependent model and suggested that the lifetime of the APN_T reservoir is often short enough compared to the timescale for changes in its production rate, that a steady-state approximation will accurately describe APN mixing ratios. In contrast to the Cleary

et al. (2007) study, which used the APN steady-state model to predict OH concentrations, the BEARPEX measurements include OH and HO_2, thus providing an opportunity to thoroughly evaluate the APN steady-state model and to test the mechanisms of PA radical production.

2 Experimental

2.1 Site description

BEARPEX 2007 took place at a site on a ponderosa pine plantation owned and managed by Sierra Pacific Industries and adjacent to the University of California Blodgett Forest Research Station (UC-BFRS). The site is located 75 km northeast of Sacramento, CA (1315 m a.s.l., 38.9° N, 120.6° W). The experiment began on 15 August 2007 and ended on 10 October 2007.

Typical meteorological conditions at the site have been described in detail previously (Lamanna and Goldstein, 1999; Schade and Goldstein, 2001; Dillon et al., 2002; Kurpius and Goldstein, 2003; Holzinger et al., 2005; Cahill et al., 2006; Farmer et al., 2006; Day et al., 2008, 2009). Briefly, the meteorology during the dry season (May-September) is typified by high daytime temperatures, low rainfall, low humidity, clear skies, and extremely regular east/west, upslope-downslope winds. During the wet season (October–April), winds are less regular, temperatures are cooler, and there is moderate rainfall and snowfall (Goldstein et al., 2000). September 2007 was cooler than typical and there were early snows in October 2007.

Daytime winds carry anthropogenically influenced air from the Greater Sacramento Area, eastward up the slope of the Sierra Nevada. The region between Greater Sacramento and UC-BFRS is sparsely populated, and the plume develops with minor inputs from additional anthropogenic emissions as it travels towards UC-BFRS (Dillon et al., 2002; Murphy et al., 2006, 2007). The anthropogenic plume has a distinct arrival time at the measurement site in the late afternoon that changes very little from day to day. A 20–25 km wide band of oak woodlands runs parallel to the Sierra Nevada foothills and is perpendicular to the mean flow from Sacramento to UC-BFRS. In the morning, air that has relatively little urban influence passes over the forest and accumulates isoprene. This air arrives at UC-BFRS a few hours ahead of the anthropogenically influenced (but also isoprene rich) air. Local emissions from the ponderosa pines include 2-methyl-3-buten-2-ol (MBO) (Schade et al., 2000) and significant amounts of monoterpenes, sesquiterpenes, and related oxygenates (Schade et al., 1999; Holzinger et al., 2005; Bouvier-Brown et al., 2008). Compared to the large injection of isoprene by the upwind oak woodlands, local isoprene emissions are small (Dreyfus et al., 2002).

A variety of long term and episodic measurements have been ongoing at the UC-BFRS site since 1997. During BEARPEX 2007, measurements were greatly expanded over these previous experiments and included a range of anthropogenic and biogenic VOCs, OH, HO_2, NO_x and other oxides of nitrogen (NO_{yi}), peroxides, CO, O_3, CO_2, aerosol composition and physical properties, and meteorological variables. Measurements used in this analysis were made from one of two walkup observation towers located ∼10 m apart. A complete overview of the campaign is given by Cohen and Goldstein (2009).

2.2 Measurements

In this analysis we use measurements of APNs, OH and HO_2, a suite of VOCs, and NO_2. The techniques and instruments used for these measurements have been described in detail previously. Speciated APN measurements were obtained via a custom-built thermal dissociation – chemical ionization mass spectrometer (TD-CIMS) (Wolfe et al., 2007, 2009). For this instrument, air was sampled from PFA inlets mounted on the North tower at 18 m through 30 m of tubing (residence time ∼2 s) into a 19 cm length of 1/2″OD PFA tubing directly attached to the CIMS instrument and heated to 180°C. At this temperature, APNs dissociate into NO_2 and acyl peroxy radicals ($RC(O)O_2$) with >95% efficiency. The hot sample gas then immediately passes through a critical orifice into an ion-molecule reaction region held at 60 Torr, where acyl peroxy radicals react with iodide to form carboxylate anions (Villalta and Howard, 1996; Slusher et al., 2004). Ions are transmitted through a collisional dissociation chamber into a quadrupole mass spectrometer where they are mass selected and detected.

In-situ calibrations and background determinations for the TD-CIMS were performed during the campaign using a photolytic PAN source and NO injection, respectively, as described by Wolfe et al. (2009). In CIMS, calibration constants are typically assumed to be similar between a family of compounds, and previous work has shown this to be true for most APNs with the exception of MPAN (Slusher et al., 2004). Post-campaign calibrations were done at NOAA-ESRL simultaneously with a gas chromatograph electron capture detection (GC/ECD) instrument (Roberts et al., 2002) and a $NO/NO_2/NO_y$ detector (Williams et al., 2000). Absolute concentrations of PAN, PPN, and MPAN from a stable diffusion source were verified using the $NO/NO_2/NO_y$ detector. These experiments confirmed that the University of Washington TD-CIMS is equally sensitive to PAN and PPN, but less sensitive to MPAN by a factor of 4.3. This relative insensitivity to MPAN is consistent across a number of TD-CIMS instruments (Slusher et al., 2004; Turnipseed et al., 2006) and was also observed for two other TD-CIMS instruments operated during these post-campaign experiments. While the precise chemical explanation for this artifact is unknown, by comparison with the GC/ECD instrument and the $NO/NO_2/NO_y$ measurements, it was concluded that this artifact is particular to the CIMS method and not an error in the

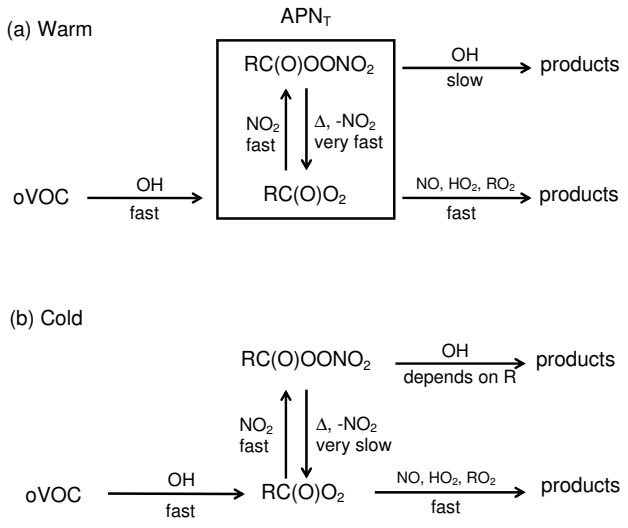

Scheme 1. 1 APN chemistry schematic under warm **(a)** and cold **(b)** conditions. APN_T is the sum of APN ($RC(O)OONO_2$) and the AP radical ($RC(O)O_2$).

characterization of the standard MPAN calibration source, synthesized according to Bertman and Roberts (1991). Thus, the PAN sensitivity was applied to all three raw APN signals to yield concentrations, and the MPAN signal was further corrected for reduced sensitivity by a factor of 4.3. The measurements are accurate to ±21% for PAN and PPN, and ±31% for MPAN, where the larger total uncertainty results from the added uncertainty of the MPAN correction factor; the precision is ±3 pptv for half-hour averaged APN concentration measurements (Wolfe et al., 2009).

Measurements of acetaldehyde, propanal, biacetyl (2,3-butanedione), methacrolein, methylvinyl ketone, isoprene and other organics were obtained on the same tower at 6 m using a 2-channel gas chromatograph/mass spectrometer (GC/MS) (Goldan et al., 2004; Bouvier-Brown et al., 2008). The accuracy of this measurement is ±25% for oxygenated species and ±15% for all other VOCs. OH and HO_2 measurements were obtained at variable heights (from 2 to 15.5 m) from a movable lift adjacent to the North tower. OH was measured by laser-induced fluorescence (LIF) at low pressure and HO_2 was converted to OH through its reaction with NO followed by the LIF detection of OH (Faloona et al., 2004). The absolute uncertainty of OH and HO_2 measurements is estimated to be 32% (2σ). NO_2 measurements were obtained by laser-induced fluorescence (Farmer et al., 2009; Fuchs et al., 2009), sampling at a height of 12 m, also on the North tower. The accuracy of the LIF NO_2 measurements during BEARPEX is estimated to be 10%. Meteorological and ozone instrumentation is located on the South tower and is described in detail elsewhere (Goldstein et al., 2000). For our analysis we rely on photosynthetically active radiation (PAR) and temperature.

Unless otherwise noted, all data used in this analysis are 30 min averages of measurements and obtained between the hours of 12:00 and 17:00 PST, when observed oVOC concentrations are relatively constant. Concurrent measurements of all observations are available from 1 September 2007 to 24 September 2007, except for short periods where one or more instruments were offline for maintenance. Subsets of the measurements are available from 15 August 2007 to 10 October 2007.

3 Kinetics of APNs

3.1 Steady-state model of APNs

The chemistry of APNs and their corresponding AP radicals are summarized by Schemes 1a–b.

Concentrations of APN_T can be calculated by explicit integration of its production and loss rates as defined by Reaction (R1a) and Reactions (3–6), respectively (Eq. 1). Note that Reactions (R2a) and (R2b) are equilibration reactions within APN_T and do not lead to net loss or gain of APN_T, and, as such, are not included in Eq. (1).

$$[\mathrm{APN}_T] = \int \{k_1[\mathrm{OH}(t)][\mathrm{oVOC}(t)] - k_3[\mathrm{AP}(t)][\mathrm{NO}(t)]\} - k_4[\mathrm{AP}(t)][\mathrm{HO}_2(t)] - k_5[\mathrm{AP}(t)][\mathrm{RO}_2(t)] \{-k_6[\mathrm{APN}(t)][\mathrm{OH}(t)]\} dt \quad (1)$$

Regardless of the thermal decomposition rate of APN, the AP radical can usually be treated in steady-state since its lifetime is very short ($\tau \sim$ 0 s) relative to typical changes in [oVOC]. [AP], therefore, can be calculated by Eq. (2).

$$[\mathrm{AP}]_{ss} = \frac{k_1[\mathrm{OH}][\mathrm{oVOC}] + k_{2b}[\mathrm{APN}]}{k_{2a}[\mathrm{NO_2}] + k_3[\mathrm{NO}] + k_4[\mathrm{HO_2}] + k_5[\mathrm{RO_2}]} \quad (2)$$

The expression for $[APN_T]$ (Eq. 3) can be simplified by combining Eqs. (1 and 2) and introducing the term, βg Eq. (4), which has a value between 0 and 1 that represents the probability that the AP radical will react with NO_2, to give an APN, over an irreversible reaction with NO, HO_2, or RO_2, to give other products (Roberts et al., 2001). The lifetime of APN_T, therefore, is dependent not only upon the thermal decomposition of the APN, but also the value of β. Equation (3) can be used to accurately calculate $[APN_T]$, provided one has knowledge of the temporal variation of the oVOC source molecule, β, and OH.

$$[\mathrm{APN}_T] = \int \{\beta(t)k_1[\mathrm{OH}(t)][\mathrm{oVOC}(t)] - (1-\beta)k_{2b}(t)\} \{[\mathrm{APN}(t)] - k_6[\mathrm{APN}(t)][\mathrm{OH}(t)]\} dt \quad (3)$$

$$\beta = \frac{k_{2a}[\mathrm{NO_2}]}{k_{2a}[\mathrm{NO_2}] + k_3[\mathrm{NO}] + k_4[\mathrm{HO_2}] + k_5[\mathrm{RO_2}]} \quad (4)$$

When APN_T is in steady-state with its sources and sinks, Eq. (3) can be further simplified as shown in Eq. (4) where

we also note that when [AP]≪[APN], [APN] is approximately equal to [APN_T].

$$[\text{APN}] \cong [\text{APN}_T] = \frac{\beta k_1 [\text{OH}][\text{oVOC}]}{k_{2b}(1-\beta)+k_6[\text{OH}]} \quad (5)$$

The relationship between the steady-state (Eq. 5) and time-dependent (Eq. 3) models was discussed by Cleary et al. (2007). Equation (4) is a good approximation of Eq. (3) when changes in the APN_T loss and production rates are small on the time scale of the APN_T lifetime. To demonstrate, we integrate Eq. (3) to give Eq. (5), subject to assumptions that OH and β are constant with time. Equation (5) describes the time-dependent behavior for a hypothetical APN, APN_A, having a precursor, $oVOC_A$. $[APN]_o$ and $[oVOC]_o$ in Eq. (5) are the initial concentrations in the model (at t=0). The dependence of APN_{TA} on the history of $oVOC_A$ is contained in the term: $(1-P/L)\times k_{1A}[OH]$, where P/L is the ratio of $oVOC_A$ production to loss and $oVOC_A$ loss is presumed to be exclusively via OH reaction. When P/L is 0 (i.e. when P=0), $[oVOC_A]$ is decreasing exponentially according to its reaction with [OH]. When P/L=1 (i.e. P=L), production balances loss and $[oVOC_A]$ is constant with time.

$$[\text{APN}_{T_A}] = \frac{\beta k_{1A}[\text{OH}][\text{oVOC}_A]}{k_{2b}(1-\beta)+k_6[\text{OH}]-(1-\frac{P}{L})k_{1a}[\text{OH}]} \left[1-e^{t((1-\frac{P}{L})k_{1A}[\text{OH}]-k_{2b}(1-\beta)-k_6[\text{OH}])}\right] + [\text{APN}_{T_A}]_0 \frac{[\text{oVOC}_A]}{[\text{oVOC}_A]_0} e^{t((1-\frac{P}{L})k_{1A}[\text{OH}]-k_{2b}(1-\beta)-k_6[\text{OH}])} \quad (6)$$

Note that Eq. (5) is modified slightly from that used by Roberts et al. (2001) who assume in all cases an exponential decay in oVOC concentrations from the point of emissions, giving P/L=0. Typical oVOC precursors of APNs, such as acetaldehyde, methacrolein, and propanal, are produced as a result of VOC-HO_x-NO_x cycling on the timescale of hours. Calculations show that P/L≠0 for these APN precursors, at least in the near-field (tens of km) with respect to VOC emission sources (see Sect. 5).

In accord with the findings of Cleary et al. (2007) it can be seen that in the case where P/L=1, the time-dependent equation takes the form of the instantaneous steady-state equation (Eq. 6) at the limit of t=∞. However, in the case where P/L=0, the lifetime of $oVOC_A$ is often short enough that the APN_T production term is decaying rapidly relative to the lifetime of APN_{TA}. In this case, there will be significant deviations between a time-dependent solution for $[APN_{TA}]$ and an approximation based on steady-state assumptions, even as t approaches infinity. This dependence on the behavior of oVOCs is reduced as the APN_T lifetime gets shorter. We also find that steady-state conditions are more likely to apply to the APN_T system when temperatures are high and thermal decomposition is fast.

3.2 Steady-state model of APN concentration ratios

It is commonly assumed that the APN thermal decomposition rate constant (k_{2b}) and the reactivity of acyl peroxy radicals (k_3, k_4, and k_5) are relatively independent of the identity of the APN alkyl group. Kirchner et al. (1999) report differences of order 25% across a series of acyl peroxy nitrates. Given this similar reactivity, it can be instructive to analyze the ratios of APNs to gain insight into the behavior of their oVOC sources. Applying the steady-state equation (Eq. 5) to the concentration of two different APNs, we derive an expression (Eq. 7) for the ratio of APN_{TA} to APN_{TB}.

$$\frac{[\text{APN}_{T_A}]}{[\text{APN}_{T_B}]} = \frac{k_{1A}[\text{oVOC}_A]}{k_{1B}[\text{oVOC}_B]} \times \frac{(1-\beta)k_{2bB}+k_{6B}[\text{OH}]}{(1-\beta)k_{2bA}+k_{6A}[\text{OH}]} \quad (7)$$

This expression can be further simplified, with the assumption that k_{2b} is identical for both APNs and that loss of both APNs by reaction with OH occurs at rates that are each much slower than the loss to reaction with NO, HO_2, and RO_2 (given by (1-β) k_{2b}). With these assumptions, the second term in Eq. (6) cancels and the ratio is approximately Eq. (7).

$$\frac{[\text{APN}_{T_A}]}{[\text{APN}_{T_B}]} \approx \frac{k_{1A}[\text{oVOC}_A]}{k_{1B}[\text{oVOC}_B]} \quad (8)$$

Analysis of Eqs. (6 and 7) indicates that APN ratios are primarily dependent on the ratio of their oVOC precursors. In addition, APN ratios will be accurately predicted as long as the ratio of the precursor oVOCs is not changing rapidly relative to the APN_T lifetimes (e.g. the steady state assumptions for APN_T ratios are accurate) and as long as the rate of APN loss to OH (Reaction R6) is slow relative to thermal decomposition followed by loss of the AP radical. Calculations indicate that this result holds over a wider range of temperatures and source conditions than was described by Cleary et al. (2007) for absolute concentrations.

As with absolute concentrations, these assumptions about a steady-state approximation for APN ratios can be tested by comparing the instantaneous steady-state equation (Eq. 7) with numerical integration of the time-dependent equations for two hypothetical APNs, APN_A and APN_B. For simplicity, we assume that both APNs each have single oVOC precursors, that both do not have any appreciable loss to reaction with OH, that their decomposition rates are identical, and that initial APN_T concentrations are 0. Under these conditions, the time-dependent ratio of APN_{TA} to APN_{TB} will be described by Eq. (8).

$$\frac{[\text{APN}_{T_A}]}{[\text{APN}_{T_B}]} = \frac{k_{1A}[\text{oVOC}_A]}{k_{1B}[\text{oVOC}_B]} \times \frac{k_{2b}(1-\beta)-(1-\frac{P}{L})k_{1B}[\text{OH}]}{k_{2b}(1-\beta)-(1-\frac{P}{L})k_{1A}[\text{OH}]} \times \frac{1-e^{t((1-\frac{P}{L})k_{1A}[\text{OH}]-k_{2b}(1-\beta))}}{1-e^{t((1-\frac{P}{L})k_{1B}[\text{OH}]-k_{2b}(1-\beta))}} \quad (9)$$

This time-dependent ratio is dependent upon the ratio of source terms, as in Eq. (7), but it is also sensitive to OH concentrations, β and to temperature when k_{1A} and k_{1B} are appreciably different and when P/L≠1. However, when P/L=1

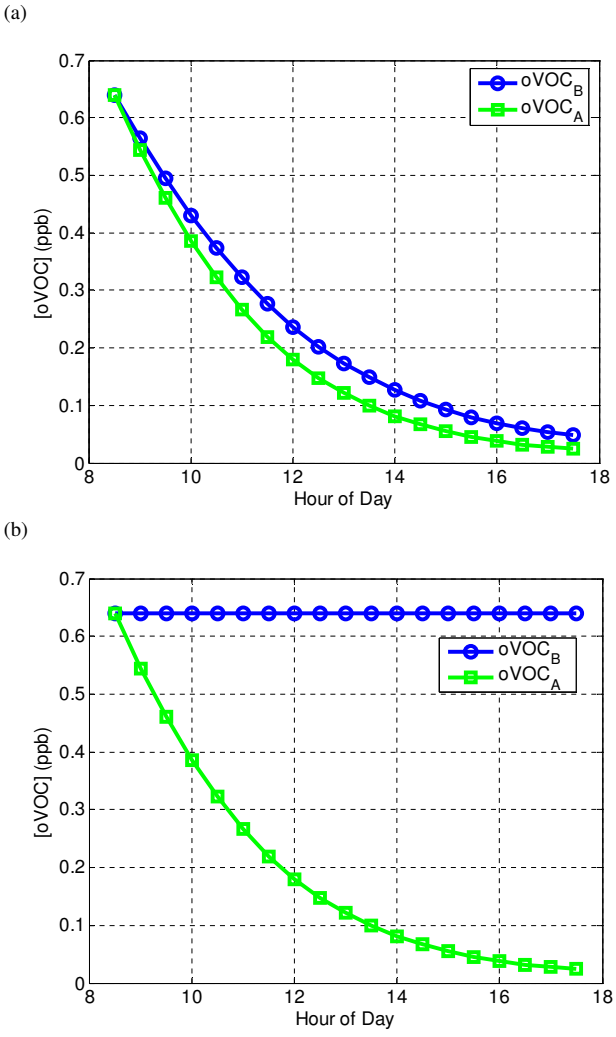

Fig. 1. oVOC profiles for time-dependent simulations of APNs: **(a)** Case A: both oVOCs decreasing exponentially with e-folding lifetimes of ∼2.5 ($oVOC_A$) and ∼3.5 h ($oVOC_B$) with no production (P/L=0) and **(b)** Case B: $oVOC_A$ decreasing as in scenario A, and $oVOC_B$ having equal production and loss rates (P/L=1).

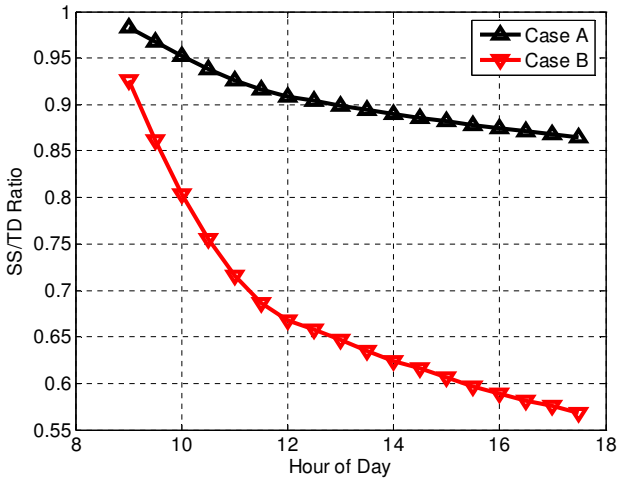

Fig. 2. Ratio of results from steady-state (SS) to time-dependent (TD) model for predicting the ratio of APN_A/APN_B for the two different cases of oVOC behavior described in the text and illustrated in Fig. 1a–b.

for both oVOCs or if the differences in k_{1A} and k_{1B} are offset by differences in $(P/L)_A$ and $(P/L)_B$ Eq. (8) reduces to the steady-state approximation (Eq. 8) at t=∞. Thus, if $oVOC_A$ and $oVOC_B$ have similar sources and sinks, the ratio of APN_{TA} to APN_{TB} is accurately approximated by the steady-state equation.

The effect of differences in the relative behavior of the oVOCs on APN ratios is illustrated with two examples: (A) both oVOC precursors are allowed to decrease exponentially due to their loss to OH (Fig. 1a) and (B) $oVOC_A$ decreases exponentially and $oVOC_B$ remains constant (Fig. 1b). In case A, at equilibrium (t=∞), the agreement between steady-state and time-dependent predictions is determined by the ratio of rate constants k_{1A} and k_{1B}, but only to the extent that this ratio changes the $[oVOC_A]/[oVOC_B]$ ratio on a time scale that is of the same order as APN_T loss. In case B, the added production of $oVOC_B$ causes a change in the $oVOC_A/oVOC_B$ ratio with time, with effects on APN_T ratios that depend on the lifetime of APN_T.

To demonstrate, we use a case where APN_T lifetimes are about 70 min, and k_{1a} and k_{1b} are equal to the rate constants for propanal and acetaldehyde (see Table 1), respectively. We initialize the time-dependent model at 9am, and the variables $[HO_2]$, $[RO_2]$, [NO], $[NO_2]$, [OH], and T are given diurnal behavior typical of the UC-BFRS measurement site. The results are shown in Fig. 2, where the steady-state predictions of APN_{TA}/APN_{TB} are plotted relative to the time-dependent predictions versus time of day. By noon, the system reaches a stationary state and remains there until about 17:00, at which time β is changing rapidly. For both cases, at all times of day, the steady-state to time-dependent ratio is seen diverging from 1 as a result of a continuously changing ratio of $oVOC_A$ to $oVOC_B$. While the system never reaches the exact steady-state, the differences are tolerable when the divergence from steady-state is slow. For example, in Case A, the steady-state model for APN_{TA}/APN_{TB} is lower than the time-dependent model by 10–15% throughout the afternoon. Case A, which represents a scenario where two oVOC precursors have similar production and loss terms, is likely, therefore, to result in a steady-state prediction of APN_T ratios that is accurate to 15%. When the behavior of oVOCs is very different, however, the agreement between time-dependent and steady-state predictions of the ratio worsens. As shown in Fig. 2, the steady-state model is in agreement with the time dependent one to within about 35–45% in Case B. From this analysis, we conclude that an e-fold change in the oVOC ratio over

150 min will result in a steady-state approximation accurate to 45% or better when the APN_T lifetimes are 70 min. A faster change in oVOC ratios would become tolerable with a corresponding decrease in APN_T lifetime.

If we now consider a third APN, APN_C, which has an appreciable loss rate to reaction with OH, the time-dependent model for the ratio of APN_{TC} to APN_{TA} or APN_{TB} will become more sensitive to the individual rates of change of each oVOC precursor, as opposed to changes in the oVOC ratios. This results from the lack of cancellation of the loss terms for the two APNs in Eq. (8). Steady-state predictions of absolute concentrations of APN_{TC} will be more accurate due to the shorter APN_{TC} lifetime, but the accuracy of the steady-state model in predicting APN_{TC}/APN_{TA} and APN_{TC}/APN_{TB} may be degraded. For comparison to the scenarios above, we assume the same conditions as in cases A and B and that the loss of APN_C to OH is about 40% of the total APN_T loss rate ($\tau_{R6}\sim$90 min and $\tau_{R2b+R35}\sim$70 min). Although the above analysis suggests some degradation of the accuracy of the steady-state approximation for the ratio, we find the steady-state predictions of ratios of APN_{TC}/APN_{TA} or APN_{TC}/APN_{TB} (Eq. 7) to be within 10% of the predictions for APN_{TA}/APN_{TB} in both cases A and B.

Our conclusions on the accuracy of the steady-state model under these various scenarios of oVOC behavior are summarized in Table 2.

3.3 Application of the steady-state model to MPAN, PPN, and PAN at UC-BFRS

Application of the steady-state model to specific APNs requires defining the production and loss terms for each APN.

3.3.1 MPAN, PPN, and PAN loss

Three important reactants for acyl peroxy radicals are NO, HO_2, and organic peroxy radicals (RO_2). NO concentrations are inferred by assuming a photo-stationary state relationship between NO_2, ozone, and peroxy radicals (HO_2+RO_2) through the following equation:

$$[NO]=\frac{J_{NO_2}[NO_2]}{k_{HO_2+NO}[HO_2]+k_{RO_2+NO}[RO_2]+k_{NO+O_3}[O_3]} \quad (10)$$

The photolysis rate of NO_2 (J_{NO2}) is obtained from the TUV model (Madronich, 1987), calculated with varying solar zenith angles at half hour intervals over the entire campaign while holding other parameters constant (cloud optical depth=0; aerosol optical depth=0.235; ozone column=300 Dobson units; single scattering aerosol albedo=0.990). The model output was scaled by measured PAR to account for the occasional periods of cloud cover. The rate constants used for calculating [NO] are listed in Table 1.

RO_2 concentrations are estimated through a separate steady-state relationship where production occurs from the reaction of OH with a suite of VOCs and loss is due to reaction with NO, HO_2, and other RO_2 radicals. This relationship leads to Eq. (10), which can be reduced to a quadratic equation.

$$[RO_2]=\frac{\sum_i k_i[OH][VOC_i]}{k_{HO_2+RO_2}[HO_2]+k_{NO+RO_2}[NO]+2k_{RO_2+RO_2}[RO_2]} \quad (11)$$

Equations (9 and 10) are solved iteratively until values of NO and RO_2 are obtained with convergence criteria of $<$1% precision. An uncertainty of a factor of 2 in either RO_2 or NO concentrations propagates into an additional uncertainty of 15–20% in the other radical.

Thermal decomposition rates of PAN and MPAN are considered to be the same in this analysis. Decomposition of PPN, however, is measured to be 25% slower (at 298 K and 1 atm) by Kirchner et al. (1999). Reactions of acyl peroxy radicals (with NO, NO_2, HO_2, or RO_2) are generally considered to be independent of R group (Roberts and Bertman, 1992). An additional difference in the chemical removal of the various APNs is reaction with OH. Of the three APNs that we are considering, only MPAN has an appreciable loss rate to reaction with OH ($\tau\sim$2 h for [OH]=5×10^6 molecules cm^{-3}), stemming from an alkene moiety (Orlando et al., 2002). PPN and PAN, in contrast, have lifetimes on the order of weeks to months with respect to 5×10^6 molecules cm^{-3} OH. APN_T deposition velocities are on the order of 10^{-1} cm s^{-1} ($\tau_{dep}\sim$20–100 h) (Wolfe et al., 2009), making deposition a 2–6% per hour sink, small enough to neglect in this analysis.

3.3.2 MPAN, PPN, and PAN production

Production of $MPAN_T$ occurs by abstraction of the aldehydic hydrogen from methacrolein during reaction with OH, followed by the effectively instantaneous addition of O_2. Equation (12), then, describes $MPAN_T$ production rate:

$$P(MPAN_T)=\alpha_{macr}k_{1macr}[OH][MACR], \quad (12)$$

where α represents the aldehydic abstraction branching ratio from the reaction of methacrolein (MACR) with OH (α_{macr}=0.45) and k_{1macr} represents the rate coefficient for the total reaction of OH+MACR.

Similarly, production of PPN_T occurs from the abstraction of the aldehydic hydrogen from propanal. The branching ratio for this process ($\alpha_{propanal}$) is $\sim$1 since the aldehydic H is the only appreciably reactive functionality.

$$P(PPN_T)=\alpha_{propanal}k_{1propanal}[OH][propanal] \quad (13)$$

Production of PAN_T occurs upon oxidation of acetaldehyde (acetal) (Carter, 1990), methyl glyoxal (MGLY) (Romero et al., 2005; Baeza-Romero et al., 2007), methacrolein (MACR) (Orlando et al., 1999), and methylvinyl ketone (MVK) (Tuazon and Atkinson, 1989), and through the photolysis of biacetyl (biacet) (Carter, 1990; Klotz et al., 2001).

Table 1. Rate constants used in analysis.

	$k(T)$ or $k(T,[M])$[a]	k(298 K)	α[b]	Reference
VOC+OH reactions				
methacrolein	8.0×10^{-12}exp(380/T)	2.9×10^{-11}	0.45	(Atkinson et al., 2006)
acetaldehyde	4.4×10^{-12} exp(365/T)	1.5×10^{-11}	1	(Atkinson et al., 2006)
propanal	5.1×10^{-12} exp(405/T)	2.0×10^{-11}	1	(Atkinson et al., 2006)
methyl glyoxal	1.83×10^{-12} exp(560/T)	1.2×10^{-11}	1	(Baeza-Romero et al., 2007)
methyl vinyl ketone	2.6×10^{-12} exp(610/T)	2.0×10^{-11}	N/A	(Atkinson et al., 2006)
Acyl Peroxy Radical reactions				
$RCOO_2+NO_2\longrightarrow$ APN (R2a)	$k_0=2.7\times10^{-28}$ (T/300)$^{-7.1}$ $k_\infty=1.2\times10^{-11}$(T/300)$^{-0.9}$ F_{cent}=0.3 N=1	1.0×10^{-11}	N/A	(Atkinson et al., 1997, 2004)
APN$\longrightarrow RCOO_2+NO_2$ (R2b)	$k_0=4.9\times10^{-3}$ exp(−12 100/T) $k_\infty=4.0\times10^{16}$exp(−13 600/T) F_{cent}=0.3 N=1.41	4.6×10^{-04}	N/A	(Atkinson et al., 1997, 2004)
PPN$\longrightarrow C_2H_5COO_2+NO_2$	$k_0=1.7\times10^{-3}$ exp(-11 280/T) $k_\infty=4.0\times10^{16}$ exp(−13 940/T) F_{cent}=0.36 N=1.41	4.6×10^{-04}	N/A	(Kirchner et al., 1999)
$RCOO_2+NO\longrightarrow$products (R3)	8.1×10^{-12} exp(270/T)	2.0×10^{-11}	N/A	(Atkinson et al., 1997, 2004)
$RCOO_2+HO_2\longrightarrow$ products (R4)	4.3×10^{-13} exp(1040/T)	1.4×10^{-11}	N/A	(MCM, 2003)
$RCOO_2+RO_2\longrightarrow$ products (R5)	2.0×10^{-12} exp(500/T)	1.1×10^{-11}	N/A	(Tyndall, 2001)
APN+OH reactions				
PAN	N/A	3×10^{-14}	N/A	(Talukdar et al., 1995)
PPN	N/A	3×10^{-13}	N/A	Estimated from (Carter and Atkinson, 1985)
MPAN	N/A	32×10^{-12}	N/A	(Orlando et al., 2002)
HOx and NOx reactions				
HO_2+RO_2	2.9×10^{-13} exp(1300/T)	2.3×10^{-11}	N/A	(MCM, 2003)
RO_2+RO_2	N/A	2.4×10^{-12}	N/A	(MCM, 2003)
$NO+RO_2$	2.54×10^{-12} exp(360/T)	8.5×10^{-12}	N/A	(MCM, 2003)
$NO+HO_2$	3.5×10^{-12} exp(250/T)	8.1×10^{-12}	N/A	(NASA, 2006)
$NO+O_3$	3.0×10^{-12} exp(−1500/T)	2.0×10^{-14}	N/A	(NASA, 2006)

[a] Where $k(M)=\frac{k_0[M]}{1+\frac{k_0[M]}{k_\infty}}\times F_c$ and $\log(F_c)=\frac{\log(F_{cent})}{1+\left(\frac{(\log k_0[M]\ k_\infty)}{N}\right)^2}$.

[b] α is the branching ratio for aldehydic abstraction.

Table 2. Summary of conclusions from comparison of steady state and time dependent models.

Upwind behavior of oVOCs			Accuracy of steady state model					
$oVOC_A$	$oVOC_B$	$oVOC_C$	APN_A	APN_B	APN_C	APN_A/APN_B	APN_C/APN_A	APN_C/APN_B
constant	constant	constant	±10%	±10%	±10%	±10%	±10%	±10%
decreasing	decreasing	decreasing	−60%	−60%	−60%	±15%	±25%	±25%
decreasing	constant	decreasing	−60%	±10%	−60%	−45%	±25%	−55%

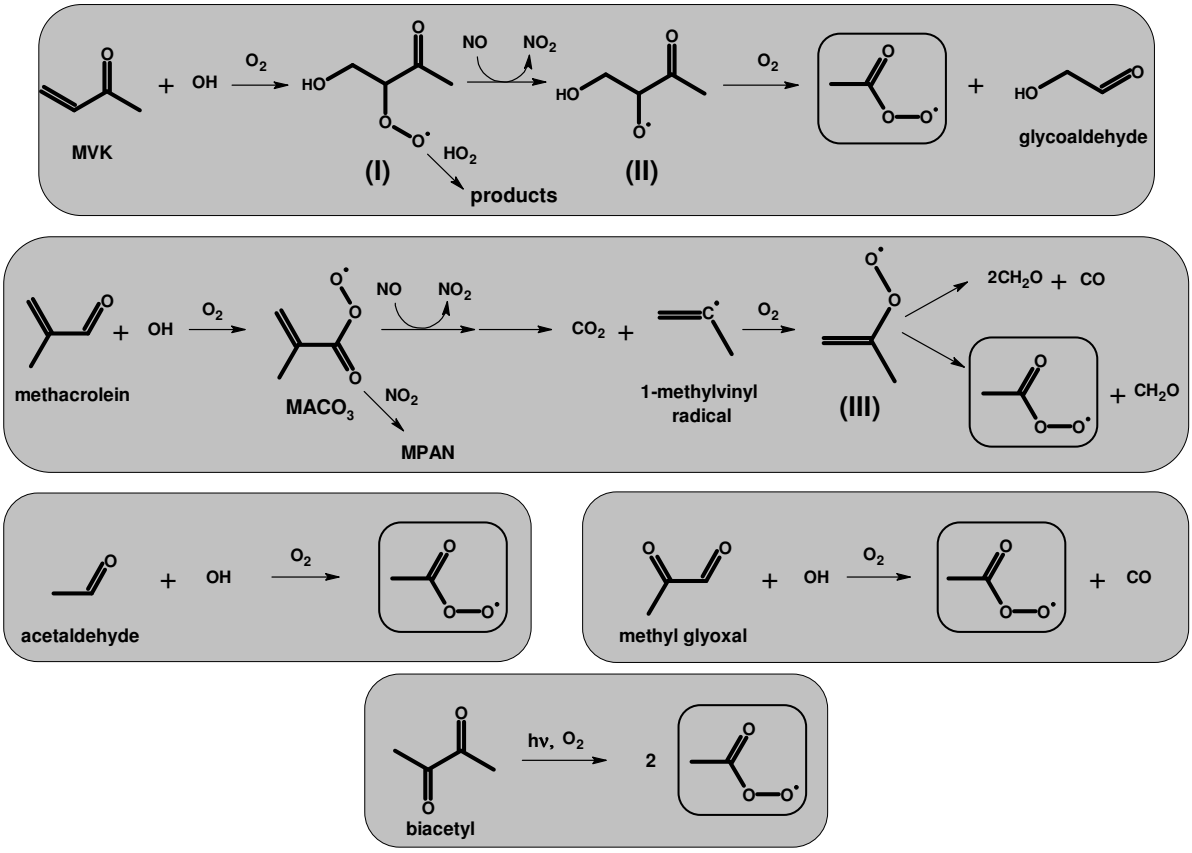

Scheme 2. Reaction mechanisms for the production of the peroxy acetyl radical (PA), which is outlined by a box in each case.

The pathways to PA radical from these five compounds are shown in Scheme 2.

The abstraction of the aldehydic H (α_{acetal}=1) from acetaldehyde by reaction with OH leads to the PA radical:

$$PA_{acetal} = \alpha_{acetal} k_{1acetal} [OH][acetal] \quad (14)$$

Reaction of MGLY with OH (Baeza-Romero et al., 2007) occurs almost exclusively via abstraction of the aldehydic H (α_{mgly}=1), and the corresponding acyl radical promptly decomposes to yield an energized acetyl radical and CO. After relaxation, the acetyl radical reacts with O_2 to form the PA radical, and PA_{mgly} is quantified as follows:

$$PA_{mgly} = \alpha_{mgly} k_{1mgly} [OH][MGLY] \quad (15)$$

We assume that the acetyl radical produced from the decomposition of the MGLY+OH reaction product gives the PA radical exclusively in the presence of O_2, however, there is some evidence for a lower PA yield because the energized acetyl radical product decomposes into CO and CH_3 at 40% yield (Baeza-Romero et al., 2007). Photolysis of MGLY can also lead to PA production, and the rate of PA production from MGLY+hν (Staffelbach et al., 1995) is expected to be similar to the actual rate of OH oxidation at [OH]=5×10^6 molec cm^{-3}. By neglecting MGLY+hν and using unity yield of PA from the MGLY reaction with OH, we introduce compensating errors that result in a reasonable approximation of PA_{mgly}.

The PA production from MVK (Tuazon and Atkinson, 1989) starts from the reaction of OH with MVK at the terminal carbon of the carbon-carbon double bond at 70% yield (Tuazon and Atkinson, 1989), producing a hydroxy peroxy radical (species I, Scheme 2). Reaction of the peroxy radical with NO yields an alkoxy radical (species II), the O_2 initiated decomposition of which produces a PA radical and glycoaldehyde, another 2nd generation isoprene oxidation product. The major competing pathway for the peroxy radical is the radical chain terminating reaction with HO_2. The reaction of the MVK-derived peroxy radical with RO_2 can also lead to production of species II with an estimated yield of 60% (Jenkin et al., 1997), with the remaining yield corresponding to products that are inconsequential to PA radical production. It was determined that for this analysis, this RO_2 chemistry has a negligible impact on the estimated PA radical production and it is ignored here. Similarly, alkyl nitrate formation (<10% yield) is also expected to have a negligible impact on the calculation of PA_{mvk}. Thus, the branching ratio for production of the alkoxy radical can be estimated as the

rate of its reaction with NO relative to its total loss rate from reactions with NO and HO_2. Decomposition of the alkoxy radical leads to the formation of glycoaldehyde and PA radical. The PA source from MVK is thus given by:

$$PA_{\mathrm{mvk}}=0.7\times k_{1\mathrm{mvk}}[\mathrm{OH}][\mathrm{MVK}]\frac{k_{\mathrm{RO2+NO}}[\mathrm{NO}]}{k_{\mathrm{RO2+NO}}[\mathrm{NO}]+k_{\mathrm{RO2+HO2}}[\mathrm{HO_2}]} \quad (16)$$

The MACR pathway to the PA radical (Orlando et al., 1999) proceeds through the same acyl peroxy radical that produces MPAN ($MACO_3$). But if the $MACO_3$ radical reacts with NO instead of reacting with NO_2 to form MPAN, the resulting alkoxy radical decomposes to give CO_2 and the 1-methylvinyl radical (MVR). MVR quickly forms an O_2 adduct (species III) which either decomposes or reacts with NO. Decomposition of the MVR-O_2 adduct proceeds via two possible pathways: one forming two formaldehyde (CH_2O) molecules and CO or one giving CH_2O and the PA radical. The yield of the CO channel was determined to be 65% by Orlando et al. (1999). MVR-O_2 reaction with NO also leads to PA radicals and CH_2O. The yield for PA radical production from the MVR-O_2 adduct, therefore, is taken as 35%, regardless of NO concentration (Orlando et al., 1999).

The calculation of PA_{macr} depends on the rate of $MACO_3$ reaction with NO and the branching ratio of the MVR-O_2 adduct decomposition. The $MACO_3$ concentration can be calculated directly from the steady-state equation (Eq. 2) for AP radicals. The equation for PA_{macr} is:

$$\mathrm{PA_{macr}}=0.35\times k_3[\mathrm{MACO_3}][\mathrm{NO}] \quad (17)$$

Acetone is known to form PA radical through photolysis (Blitz et al., 2004), however, its lifetime of ∼60 h in the lower troposphere is too long to be relevant for the current analysis. Likewise, photolysis of MACR ($\tau\sim$50 h) and MVK (τ=59 h) are also too slow (Gierczak et al., 1997) to be a significant fraction of total PA production at UC-BFRS. An additional pathway that is likely to be significant is the photolysis of biacetyl (2,3-butanedione), which leads to the production of two PA radicals as shown in Scheme 2 (Klotz et al., 2001). We use a suggested scaling factor relative to J_{NO2} (3.64%) for the biacetyl photolysis rate (J_{biacet}) (Klotz et al., 2001). PA production from biacetyl is then:

$$\mathrm{PA_{biacet}}=2\mathrm{J_{biacet}}[\mathrm{biacetyl}] \quad (18)$$

3.3.3 Transport and mixing

This analysis is greatly simplified due to the constant transport patterns between Sacramento and UC-BFRS. Both biogenic and anthropogenic species arrive at UC-BFRS from the same wind direction with regularity on a daily basis, so the simple model described in Sect. 3.2 can be reasonably applied to the current data set. A Lagrangian model has been developed for the Sacramento urban plume and tested against observations, supporting these assumptions (Dillon et al., 2002; Perez, 2008; Perez and Cohen, 2009). Further, the analysis is designed such that our assumptions about the upwind behavior of APNs, oVOCs, and oxidants can be tested using the relative behavior of MPAN and PPN, compounds for which the production rates are accurately known.

Uncertainty in the current analysis, with respect to transport and mixing, could result from different entrainment rates for the different oVOCs and APNs with background air. If, for example, the entrainment rate for PAN_T or any of its precursor oVOCs are significantly different from that for $MPAN_T$ and PPN_T (due to different background concentrations), a situation could arise where $MPAN_T$ and PPN_T could be in steady-state, but not PAN_T. The entrainment rates can be estimated as $-k_{\mathrm{mix}}([\mathrm{X}]-[\mathrm{X}]_{\mathrm{bg}})$, where k_{mix} is the entrainment rate constant (determined to be 0.31 h^{-1} by Perez and Cohen, 2009) and $[\mathrm{X}]_{\mathrm{bg}}$ is the background concentration for a given species X. Using background concentrations estimated by Perez and Cohen (2009), the entrainment time constant is on the order of 4–5 h for APN_T and 5–10 h for the various oVOC precursors used in this analysis. The time scale for mixing, therefore, is likely too slow to be important at the highest temperatures, when chemical loss of APN_T ($\tau<$1 h) and oVOCs ($\tau\sim$1–2 h) are fastest. Thus, we make the assumption of equal entrainment rates and background concentrations for all APNs and oVOC precursors. Similar assumptions have been made in previous analyses of APNs (cf. Roberts et al., 2006).

4 Observations during BEARPEX

Average and maximum concentrations of all species used in this analysis, both measured and inferred, are listed in Table 3. Relative uncertainties for each species are also included. Values are given for the entire campaign and for the hot ($T>$20°C) and cold ($T<$20°C) periods of the campaign. These values are calculated only from the periods of time during which all of the relevant observations are concurrent, giving a total of 66 half-hour data points (26 during the cold period and 40 during the hot period). Over the course of the campaign, the calculated lifetimes of PAN_T and PPN_T ranged from ∼4 h at 15°C to ∼50 min at 30°C, while that of $MPAN_T$ ranged from ∼2 h to ∼25 min at these same temperatures.

4.1 Diurnal observations of APNs and oVOC precursors

As a result of the extremely small day-to-day variability of horizontal transport conditions between Sacramento and the measurement site (UC-BFRS), interpretation of diurnal patterns is instructive for understanding the biogenic and anthropogenic contributions to various species. Locally emitted biogenic VOCs, for example, often follow daytime temperature and sunlight cycles coupled to boundary layer dynamics.

Table 3. Summary of observed and inferred species for entire campaign, temperatures above 20°C, and temperatures below 20°C.

	Full Campaign (n=66)			Temperatures>20°C (n=40)			Temperatures<20°C (n=26)			
Species	mean[a]	median	max	mean	median	max	mean	median	max	accuracy (1σ)
PAN	451	392	1469	304	301	663	676	600	1469	21%
PPN	43	29	160	20	18	51	77	79	160	21%
MPAN	32	28	75	30	30	66	36	28	75	31%
Acetaldehyde	589	538	1580	677	651	1580	452	418	848	25%
Methyvinyl Ketone (MVK)	1123	1044	4087	1741	1768	4087	173	177	438	25%
Methacrolein (MACR)	334	256	1107	480	484	1107	109	121	228	25%
Biacetyl	49	49	80	57	55	80	36	35	53	25%
Methyl Glyoxal (MGLY)[b]	139	139	300	212	219	300	49	34	97	100%
NO[b]	65	55	188	57	53	99	77	72	188	100%
NO_2[c]	400	400	400	400	400	400	400	400	400	10%
OH	0.283	0.279	0.662	0.361	0.333	0.662	0.162	0.156	0.277	16%
HO_2	21	23	44	28	28	44	12	10	24	16%
RO_2[b]	82	85	223	118	113	223	28	26	48	100%
O_3 (ppbv)	57	57	83	63	65	83	47	44	71	1%

[a] All concentration units are pptv unless otherwise noted.
[b] Concentrations inferred (see text) and given a conservative factor of 2 uncertainty.
[c] Average NO_2 concentration used for entire analysis.

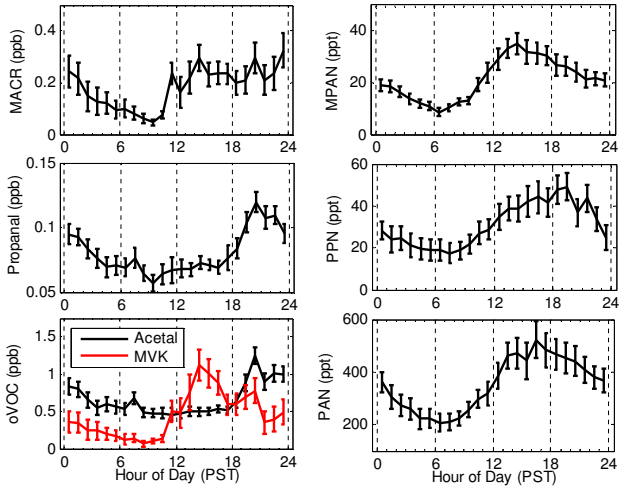

Fig. 3. Diurnal hourly medians of oVOC precursors to APNs: methacrolein, propanal, and acetaldehyde/methylvinyl ketone (acetal/MVK) (left side, top to bottom) and APNs: MPAN, PPN, and PAN (right side, top to bottom). The bars represent the 1σ variance of the mean.

Isoprene and its oxidation products typically arrive at the site around noon, after a few hours transport from the Oak forests in the foothills. The mixing ratios of anthropogenic compounds and their oxidation products which are carried from Sacramento, further upwind, peak several hours after the arrival of the isoprene plume, typically between 18:00–20:00 PST.

Average (median) diurnal concentrations of the three most abundant APNs, PAN, PPN, and MPAN, are shown in Fig. 3 (right panels) along with that of their oVOC precursors (left panels). Averages are obtained only from those times when APN and oVOC measurements were concurrent, which spanned the time period from 24 August to 27 September. The differences in the diurnal profiles of APNs can be qualitatively (and quantitatively, as we show below) explained by diurnal variations of their oVOC precursors. MPAN (Fig. 3, top right) peaks at 14:00 PST, concurrently with peak methacrolein concentrations (Fig. 3, top left), and then steadily decreases throughout the late afternoon and night. PPN (Fig. 3, middle right) rises steadily throughout the afternoon, peaking at 19:00–20:00 PST, nearly concurrently with the peak in propanal (Fig. 3, middle left). PAN (Fig. 3, bottom right) increases rapidly in the early afternoon and peaks later than the MPAN peak, but earlier than the PPN peak. This pattern is consistent with combined sources of PAN being from both biogenic and anthropogenic precursors, as shown by the diurnal profiles of MVK and acetaldehyde (Fig. 3, bottom left). Daytime (12:00–17:00 PST) average concentrations of the three APNs and their precursor oVOCs are listed in Table 3 for the full campaign as well as for the hot (T>20°C) and cold periods (T<20°C) of the measurement period.

4.2 Estimated PAN production rate

The total production rate of the PA radical is given by summing Eqs. (12–16):

$$\mathrm{P(PAN}_T\mathrm{)}=\mathrm{PA}_{\mathrm{mvk}}+\mathrm{PA}_{\mathrm{macr}}+\mathrm{PA}_{\mathrm{acetal}}+\mathrm{PA}_{\mathrm{mgly}}+\mathrm{PA}_{\mathrm{biacet}} \quad (19)$$

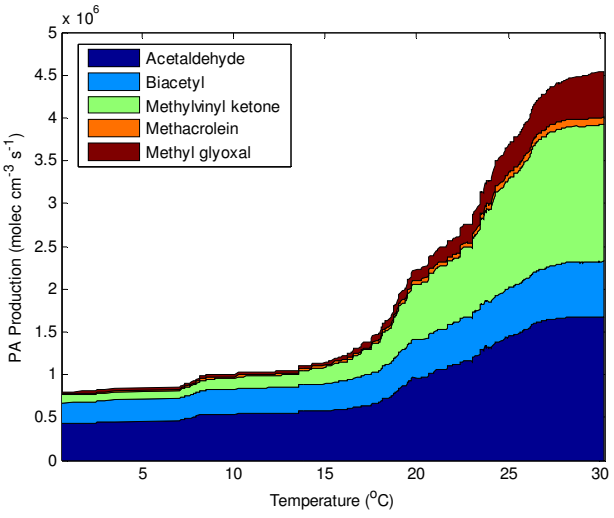

Fig. 4. Behavior of different PA production sources vs temperature. Mechanisms for each production route are shown in Scheme 2. This figure is obtained by using a running average with temperature of the calculated production rates from observations of oVOCs.

Acetaldehyde, MVK, MACR, and biacetyl were measured during BEARPEX. To calculate P(PAN_T) we use an estimate of MGLY concentrations based on MGLY observations made in August and September of 2000 at UC-BFRS by Spaulding et al. (2003). Observed concentrations ranged from 32–320 pptv, with a mean of 130 (±60) pptv. In addition to isoprene, MGLY is also an oxidation product of acetone as well as a number of aromatic species (Tuazon et al., 1986; Smith et al., 1999). Spaulding et al. (2003) used factor analysis to conclude that its sources at UC-BFRS were primarily biogenic in origin. Based on this, we give our estimated MGLY mixing ratios a simple temperature dependence to simulate a biogenic source. At 15°C and below, we use the observed nighttime background values of 30 pptv; above 15°C the concentrations follow a linear relationship:

$$[\mathrm{MGLY}]=30\ \mathrm{pptv}+\left(\frac{270\ \mathrm{pptv}}{15}\right)(T-15) \quad (20)$$

We estimate a factor of 2 uncertainty in MGLY by this equation, resulting in variations of about 10% in the PA radical production rate (P(PAN_T)).

It is instructive to view P(PAN_T) and the relative strengths of each individual source as a function of temperature (Fig. 4). The data in Fig. 4 is obtained by taking a running average of the calculated production rates, using observations of oVOCs, along the temperature coordinate. The magnitude of each PA production source increases with temperature even for non-biogenic precursors as a result of the 2–3 fold increase in the observed OH concentrations over this temperature range. Isoprene-derived sources, particularly PA_{mvk}, increase at a still more rapid rate. PA_{acetal}, however, decreases as a fraction of P(PAN_T) from about 80% at the lowest temperatures to about 35% at the highest temperatures. At temperatures above 20°C, methylvinyl ketone (PA_{mvk}) becomes the dominant non-acetaldehyde source of PA radicals, reaching about 35% of the total and 60% of the non-acetaldehyde source at the highest temperatures. Methacrolein is a relatively minor source of PA radicals at UC-BFRS. PA_{macr} is less than 4% of P(PAN_T) at any temperature. PA_{mgly} is about 10% of the total at 30°C. The photolytic biacetyl source shows a slight increase at high temperatures. Biacetyl concentrations remain relatively constant, but PA_{biacet} increases with temperature as a result of an increase in the photolysis rate on the hotter days of the campaign, which were earlier in the season and experienced slightly lower solar zenith angles. As a fraction of the total PA source, PA_{biacet} decreases with increasing temperature, ranging from about 30% to about 15% of the total, at the low and high temperature limits, respectively. A summary of these results is given in Table 4, which describes averages for the entire campaign as well as those for both high (>20°C) and low (<20°C) temperature periods. The fractional PA production rates are given for each individual source, for the lumped non-acetaldehyde sources, and for the lumped isoprene-derived sources (MVK+MACR+MGLY). The absolute PA radical production rate is also given.

5 APN_T ratio predictions

As the derivation of Eqs. (6 and 7) demonstrated, APN ratios are almost exclusively sensitive to the behavior of their source oVOCs. Figure 5 shows the dependence of the ratios MPAN/PPN (Fig. 5a), MPAN/PAN (Fig. 5b), and PPN/PAN (Fig. 5b) on temperature. MPAN/PPN and MPAN/PAN ratios increase with temperature from about 0.3 to ∼3 and 0.03 to 0.15 respectively. PPN/PAN, conversely, decreases with temperature from about 0.15 to 0.05. Qualitatively, this behavior is consistent with an increase in biogenic VOCs with temperature and with MPAN being biogenic in origin, PPN being anthropogenic in origin, and PAN having some combination of both. Also shown in Fig. 5 are the predicted ratios, calculated using Eq. (6).

In order to increase the number of calculations that can be compared to the APN_T observations, a single average value of [NO_2] is used (400 pptv), while NO is allowed to vary according to the photo-stationary state equation (Eq. 10) with inputs of HO_2, RO_2, O_3, and J_{NO2} in order to capture diurnal changes in the NO/NO_2 ratio. Our primary interest is in resolving temperature-dependent discrepancies between observations and models, which are sensitive to the NO_2/NO ratio rather than the magnitude of total NO_x. We investigated whether diurnal changes in the absolute concentration of NO_2, which has a negative correlation with temperature, are important and there was no change in our conclusions if we fix NO_2 or vary its concentration with time of day based on a diurnal average.

Table 4. Summary of PA radical sources for entire campaign, temperatures above 20°C, and temperatures below 20°C.

	Full Campaign (n[a]=66)			Temperatures>20°C (n=40)			Temperatures<20°C (n=26)		
PA Source	mean (%)	median (%)	max (%)	mean (%)	median (%)	max (%)	mean (%)	median (%)	max (%)
Acetaldehyde	45.7	41.4	89.7	36.9	37.5	54.5	59.2	57.7	89.7
Methylvinyl Ketone (MVK)	26.3	31.8	48.2	35.9	35.6	48.2	11.6	12.3	32.1
Methacrolein (MACR)	1.9	1.9	3.8	1.9	1.9	3.3	1.8	1.8	3.8
Biacetyl	19.5	17.4	56.8	15.4	13.9	33.1	25.9	23.9	56.8
Methyl Glyoxal (MGLY)[b]	6.6	8.3	13.7	9.9	9.9	13.7	1.6	1.6	5.7
Total non-acetaldehyde	54.3	58.6	80.7	63.1	62.5	80.7	40.8	42.3	69.7
Total isoprene-derived[c]	34.8	40.7	63.7	47.7	48.1	63.7	14.9	16.2	39.0
Total PA Production Rate[d]	3.0×10^6	2.6×10^6	1.2×10^7	4.4×10^6	4.2×10^6	1.2×10^7	1.0×10^6	9.1×10^5	2.4×10^6

[a] n represents the number of 30 min averaged observations for each time period.
[b] MGLY concentrations estimated from Spaulding et al. (2003) according to Eq. (20).
[c] Isoprene-derived sources include MVK, MACR, and MGLY.
[d] Production rate given in units of molecules $cm^{-3}\,s^{-1}$.

The uncertainty in the calculated APN_T ratios is estimated to be ~40% based on propagation of the uncertainties in the individual observations used in Eq. (6), a similar or larger value to the accuracy expected based on approximations used to derive the equation. The experimental uncertainty stems mainly from the uncertainty in absolute concentrations of calibration standards, and thus does not have any temperature dependence. As the APN_T ratios are mainly a function of the ratios of their production rates, uncertainty in our inferred concentrations of NO and RO_2 has only a minor effect on the APN_T ratio calculations. A factor of 2 uncertainty in both NO and RO_2 results in only a 5% increase in the APN_T ratio uncertainty.

Panels a–b in Fig. 5 show that the predicted ratios exhibit the same general behavior as the observations for all three APN_T pairs. Figure 6 shows the comparison between observed and predicted APN_T ratios along the temperature coordinate. A value of 1 in this plot corresponds to perfect agreement between observations and predictions. All data points in this figure are the averages of between 5 and 8 individual half-hour measurement-model pairs. The bars represent the $1\,\sigma$ variance of the mean for each bin. As discussed previously, the accuracy in predicting relative APN_T concentrations with the steady-state equation relies on the oVOC precursors for both APNs having similar sources and sinks, such that there are slow (relative to the APN_T lifetime) upwind changes in the oVOC ratio. The main driver of differences in oVOC behavior along the Sacramento-UC-BFRS transect is the relative importance of anthropogenic versus biogenic, and primary versus secondary sources of the oVOCs. Smaller differences arise from the different lifetimes of the oVOC precursors. The emission sources of the anthropogenic parent compounds to propanal and acetaldehyde are negligible immediately outside of Greater Sacramento (Dillon et al., 2002; Murphy et al., 2006, 2007), while the emission sources of isoprene, the parent compound to both MVK and MACR, maximize about an hour or so downwind of Greater Sacramento. In the immediate upwind vicinity of UC-BFRS, therefore, propanal and acetaldehyde are more likely to be following an exponential decay, while changes in MACR and MVK are more likely affected to some extent by local production. A useful strategy for estimating the upwind behavior of oVOCs is to calculate the instantaneous loss and production rates at UC-BFRS for each oVOC. Using observations of isoprene and OH at UC-BFRS, we find that the production rate of MVK and MACR exceeds their chemical loss rates at high temperatures by as much as a factor of 1.6 and 2.3, respectively. Production rates calculated for propanal from observations of n-propanol, and for acetaldehyde from observations of ethanol, are estimated to be only about 10% and 50%, respectively, of their loss rates to OH. In addition to chemical production, however, local emissions are likely to be an additional source of acetaldehyde at UC-BFRS (Schade and Goldstein, 2001). At an estimated flux of $0.2\,mg\,C\,m^{-2}\,h^{-1}$ at 30°C (Schade and Goldstein, 2001), emissions of acetaldehyde correspond to an atmospheric production rate similar to that expected from ethanol oxidation. Thus, acetaldehyde loss is calculated to be equal to the sum of chemical production and local emissions, with the effect that acetaldehyde is approximately in steady-state at a constant value upwind of UC-BFRS.

The predictions and observations of all three APN_T ratios are in agreement to better than 40% at temperatures above 27°C and within 25% at the highest temperature. Deviations of the steady-state predictions from observations at low temperatures can be explained by significant differences in the loss rates for $MPAN_T$ relative to PPN_T and PAN_T as a result of its fast loss to OH, which are especially apparent at low temperatures where loss to thermal decomposition for APNs is slow. Under these conditions, the steady-state Eq. (7) will not approximate the time-dependent Eq. (9). For the conditions observed during BEARPEX, Reaction (R6) becomes

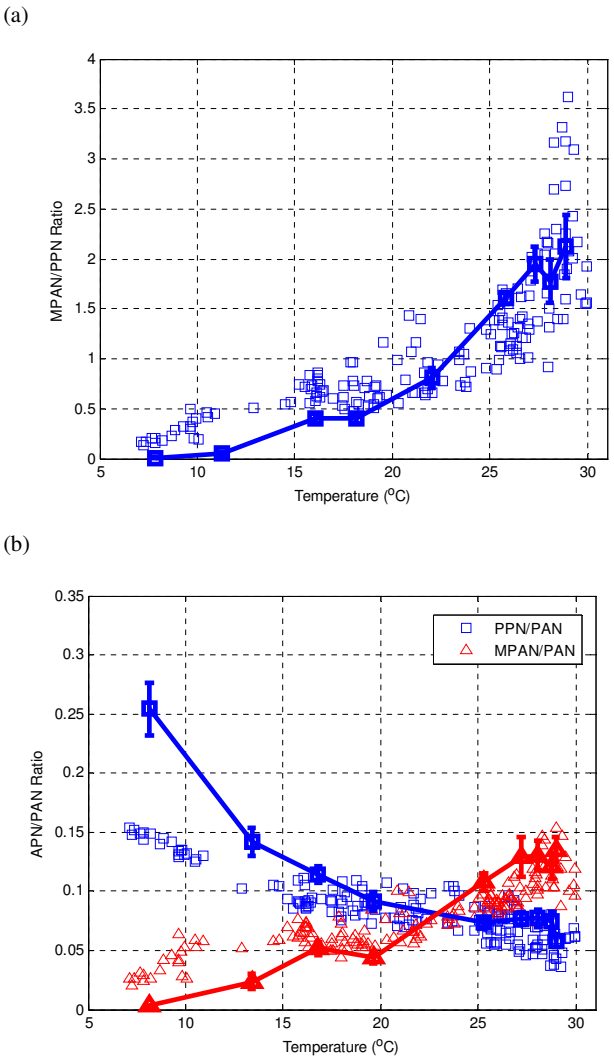

Fig. 5. Observed APN ratios vs. temperature: **(a)** MPAN/PPN (blue squares) and **(b)** MPAN/PAN (red triangles) and PPN/PAN (blue squares). Also shown are the steady-state predictions for each ratio, binned by temperature (connected symbols); the bars represent the $1\,\sigma$ variance of the predicted mean.

the dominant loss pathway for $MPAN_T$ when temperatures are below 24°C. At 30°C, Reaction (R6) accounts for about 40% of the total loss of $MPAN_T$. Therefore, the ratios involving MPAN are significantly underestimated as temperatures get colder. Similarly, since the thermal decomposition lifetime of PPN is about 30% lower than that of PAN at the lowest temperatures, the PPN_T/PAN_T ratio is significantly overestimated at these temperatures.

The uncertainty in the absolute PA radical production rate is estimated to be about 20–30%. Individual contributions to this uncertainty are largest for the MVK (10%) and acetaldehyde (9%) sources. Propagating this uncertainty through the calculation of the $MPAN_T/PAN_T$ and PPN_T/PAN_T ratios

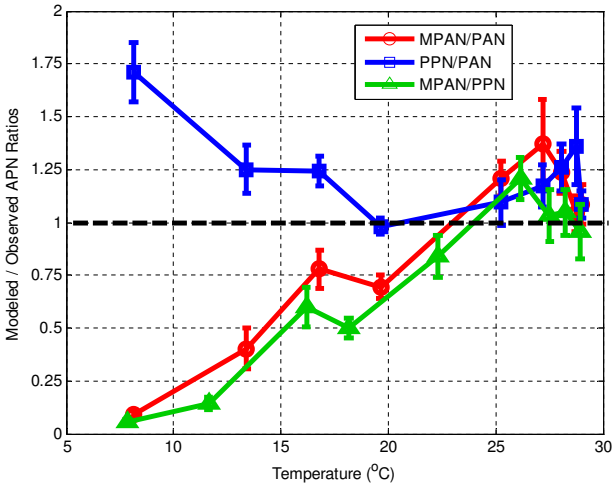

Fig. 6. Modeled-to-observed ratios for: PPN/PAN ratio (blue squares), MPAN/PAN ratio (red circles), and MPAN/PPN (green triangles). The bars represent the $1\,\sigma$ variance of the mean.

(Eq. 7) gives an overall uncertainty of 40% in the predicted APN_T ratios. Therefore, the agreement between predictions and observations, within this uncertainty, of the $MPAN_T/PAN_T$ and PPN_T/PAN_T ratios at the highest temperatures is evidence that our parameterization of PA radical production is accurate. Alternatively, it is possible that we have underestimated the production of all 3 AP radicals equally, but we dismiss this as unlikely. We estimate, therefore, based on the total uncertainty in the steady-state approximation (see Sect. 3.2), that the PA radical budget is closed to within 40%. To our knowledge, this is the first experimental study where explicit bottom-up analysis of the PA radical budget has achieved closure.

6 Absolute APN concentrations

In Sect. 5 we used APN ratios to constrain their production rates. Here we take those production rates as known values and evaluate our understanding of APN loss rates using absolute APN concentrations. Figure 7 shows the steady-state concentrations for PAN, MPAN, and PPN (Eq. 5) divided by the observations as a function of temperature. As in Fig. 6, all observations in this figure are the averages of between 5 and 8 individual half-hour measurement-model pairs, with bars representing the $1\,\sigma$ variance of the mean. As shown in Fig. 7, the modeled-to-observed ratios for all three APNs are significantly different from 1 at temperatures below 15°C. This disagreement is expected for all three APNs: both the long APN_T lifetimes at low temperatures and the dependence of the steady-state predictions on changes in absolute oVOC concentrations over this lifetime contribute to these differences. The model prediction of excess PAN and PPN implies that the rate of change in the production term exceeds the

APN_T loss rate (i.e. the exponential term in Eq. 5 is positive) at low temperature. Conversely, the prediction of too little MPAN implies that its loss rate remains fast enough (due to its reaction with OH) that it exceeds the rate of change in oVOC precursor (MACR) concentrations (i.e. the exponential term in Eq. 5 is negative).

The model agrees with observations for PAN to within 25%, for PPN to within 50%, and for MPAN to within 35% between 15°C and 20°C. Above 20°C, all three APNs are increasingly over-estimated by the model. The model for all three APNs predicts 60–100% more than is observed at temperatures greater than 27°C. This result is surprising since deviations from steady-state should approach zero (modeled-to-observed ratio=1) as temperatures rise and APN_T lifetimes decrease. While deposition is not considered in our steady-state model, its inclusion decreases the predicted APN concentrations only by ∼5% at high temperatures using the highest deposition velocity ($1.3\,cm\,s^{-1}$) reported by Wolfe et al. (2009). Additionally, the assumption that $[APN] \approx [APN_T]$ is valid since we calculate that AP radical concentrations are less than 3% of their corresponding APN over the entire campaign.

We suspect that the chemical model used to describe APN concentrations is missing a significant reactive loss channel for AP radicals. It is unknown whether this is a result of an error in our estimation of the NO, HO_2, or RO_2 loss rates or a result of neglecting some additional loss term, such as photolysis or aerosol uptake. An error in the inferred [NO], based on the NO-NO_2-O_3 photostationary-state assumptions is possible, however, previous measurements of NO and NO_2 at UC-BFRS indicate that a factor of 3 error in the NO/NO_2 ratio, required to force agreement between the APN model and observations, is unlikely at this particular site, which is far removed from significant NO_x sources (Day et al., 2009). A significant uncertainty in the model is in the estimate of the AP+RO_2 reaction rate, stemming from an uncertainty in the estimated concentrations of RO_2 (from Eq. 10) and in the reaction rate constant (k_5). We estimate that the average RO_2/HO_2 ratio is about 4, and at high temperatures, RO_2 can contribute to as much as 35% of the total AP radical loss. The rate constant used in our analysis for these reactions is that reported for the reaction of the PA radical with the methyl peroxy radical (CH_3O_2). Villenave et al. (1998) have suggested, based on experimental and theoretical considerations, that reactions of acyl peroxy radicals with any peroxy radical will proceed at a rate similar to that of PA+CH_3O_2, regardless of the size or functionality of the organic chains. The reactions of acyl peroxy radicals with hydroxy-functionalized RO_2 radicals were not specifically considered by Villenave et al. (1998), nor have they been investigated in any other experimental study, to our knowledge. This is important as the majority of peroxy radicals at UC-BFRS during the afternoon are hydroxy-peroxy radicals derived from 2-methylbut-3-en-2-ol (MBO), isoprene, terpenes, and their respective oxidation products. An increase in the rate constant for AP radicals reacting with the pool of RO_2 radicals by a factor of 3 would bring the predicted APN concentrations into agreement with observations at the highest temperatures. For comparison, the $RC(O)O_2$+HO_2 rate constant is about a factor of 1.5 higher than the $RC(O)O_2$+RO_2 rate constant.

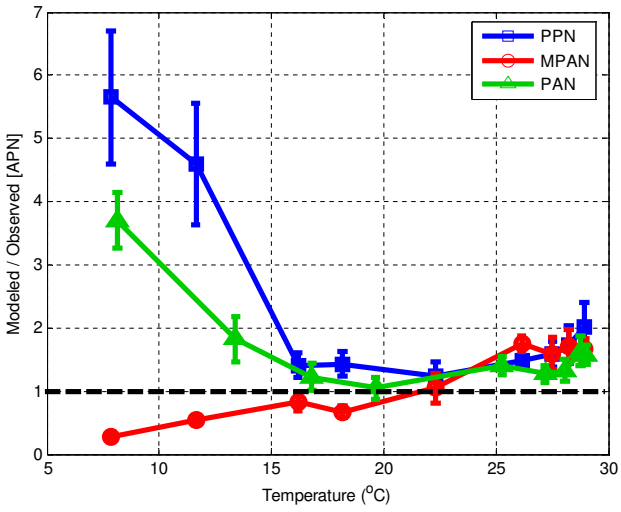

Fig. 7. Modeled-to-observed ratios for: PAN (green triangles), PPN (blue squares), and MPAN (red circles). The bars represent the 1σ variance of the mean.

An increase in the calculated RO_2 concentrations would also help explain the model bias and may be a more likely possibility since a significant increase in k_5 would lead to a lower estimate of $[RO_2]$ via Eq. (10), since the effective $k_{RO2+RO2}$ rate constant would increase. The RO_2 production term in Eq. (10) neglects direct production from carbonyl photolysis, alkene ozonolysis, and decomposition of alkoxy radicals, which may be important at UC-BFRS. Without running a detailed chemical model, which is beyond the scope of this study, it is difficult to make a better approximation for RO_2. Our estimates are, however, consistent with those resulting from an analysis of the NO-NO_2-O_3 photo-stationary state at UC-BFRS in 2001 (Day et al., 2009). While it seems unlikely that RO_2 is under estimated by a factor of 3, there is some precedent in the literature for higher observed RO_2/HO_2 ratios than our estimation during BEARPEX (Mihelcic et al., 2003; Emmerson et al., 2007).

While we believe that chemical loss of AP radicals is the most likely source of error in the model, there are other possibilities that may contribute to the observation-model differences.

We have also considered, for example, the likelihood that fast spatio-temporal variations in APN sources or sinks may be responsible for driving APNs out of steady-state. The changes required in [oVOC], β, and/or [OH] over the 5–10 km upwind of UC-BFRS are too fast to be realistic based on previous work modeling the Sacramento-UC-BFRS transect (Perez, 2008; Perez and Cohen, 2009).

7 Conclusions

We have presented an observationally constrained steady-state analysis of PAN, PPN, and MPAN. We estimate a total non-acetaldehyde source of peroxy acetyl radicals (PA), and thus PAN, that is up to ∼4 times that of acetaldehyde and find that methylvinyl ketone, methyl glyoxal, biacetyl, and methacrolein represent 63% of the total PA radical source on average at the highest observed temperatures. This is the first time that observations have confirmed the The magnitude of the inferred non-acetaldehyde PA radical source is similar to that reported as an unexplained PA radical source in other biogenically influenced observations, typically in the range of 2–3 times that of the acetaldehyde source (Roberts et al., 2001, 2006; Cleary et al., 2007). During BEARPEX 2007, values ranged from ∼0.5 to ∼4 times the calculated production from acetaldehyde and were about 1.7 times that of acetaldehyde on average at temperatures greater than 20°C. Methylvinyl ketone, an isoprene oxidation product, explains, on average, 35% of the non-acetaldehyde source when temperatures exceeded 20°C. Biacetyl can contribute 15% the total PA production under high temperature conditions, but it is most important in a relative sense when isoprene-derived sources are low. At temperatures below 20°C, acetaldehyde contributes ∼60% and biacetyl accounts for ∼25% of the total PA radical sources.

We find that the MPAN/PAN and PPN/PAN ratios can be described by a steady-state model to within 40% at temperatures greater than 15°C, thus verifying the proposed mechanisms for PA radical production. Predictions for the MPAN/PPN ratio are within 40% of observations at temperatures above 27°C. Absolute concentrations of PAN, PPN, and MPAN are all predicted to be too high by a factor of 1.6–2 at the highest observed temperatures, indicating some common bias in the steady-state model for absolute APN concentrations. We suggest that experiments aimed at measuring the rate constants of the PA radical with a series of hydroxy peroxy radicals are needed to constrain the loss rates of APNs in low NO_x/high VOC regimes.

Acknowledgements. The authors thank the UC Blodgett Forest Research Station staff for logistical support and Sierra Pacific Industries for access to their land. This work was supported by the National Science Foundation (grants ATM-0639847 (Berkeley) and ATM-0633897 (UW)). B. LaFranchi acknowledges support from the Camille and Henry Dreyfus Postdoctoral Program in Environmental Chemistry. G. Wolfe acknowledges support from NASA ESSF NNG-05GP64H.

Edited by: J. Lelieveld

References

Atkinson, R., Baulch, D. L., Cox, R. A., Hampson, R. F., Kerr, J. A., Rossi, M. J. and Troe, J.: Evaluated kinetic and photochemical data for atmospheric chemistry: Supplement VI – IUPAC subcommittee on gas kinetic data evaluation for atmospheric chemistry, J. Phys. Chem. Ref. Data, 26, 1329–1499, 1997.

Atkinson, R., Baulch, D. L., Cox, R. A., Crowley, J. N., Hampson, R. F., Hynes, R. G., Jenkin, M. E., Rossi, M. J., and Troe, J.: Evaluated kinetic and photochemical data for atmospheric chemistry: Volume I – gas phase reactions of O_x, HO_x, NO_x and SO_x species, Atmos. Chem. Phys., 4, 1461–1738, 2004, http://www.atmos-chem-phys.net/4/1461/2004/.

Atkinson, R., Baulch, D. L., Cox, R. A., Crowley, J. N., Hampson, R. F., Hynes, R. G., Jenkin, M. E., Rossi, M. J., Troe, J., and IUPAC Subcommittee: Evaluated kinetic and photochemical data for atmospheric chemistry: Volume II - gas phase reactions of organic species, Atmos. Chem. Phys., 6, 3625–4055, 2006, http://www.atmos-chem-phys.net/6/3625/2006/.

Baeza-Romero, M. T., Glowacki, D. R., Blitz, M. A., Heard, D. E., Pilling, M. J., Rickard, A. R., and Seakins, P. W.: A combined experimental and theoretical study of the reaction between methylglyoxal and OH/OD radical: OH regeneration, Phys. Chem. Chem. Phys., 9, 4114–4128, 2007.

Bertman, S. B. and Roberts, J. M.: A PAN analogue from isoprene photooxidation, Geophys. Res. Lett., 18, 1461–1464, 2001.

Blitz, M. A., Heard, D. E., Pilling, M. J., Arnold, S. R. and Chipperfield, M. P.: Pressure and temperature-dependent quantum yields for the photodissociation of acetone between 279 and 327.5 nm, Geophys. Res. Lett., 31, L09104, doi:10.1029/2004GL020182, 2004.

Bouvier-Brown, N. C., Goldstein, A. H., Worton, D. R., Matross, D. M., Gilman, J. B., Kuster, W. C., Welsh-Bon, D., Warneke, C., de Gouw, J. A., Cahill, T. M., and Holzinger, R.: Methyl chavicol: characterization of its biogenic emission rate, abundance, and oxidation products in the atmosphere, Atmos. Chem. Phys. Discuss., 8, 19707–19741, 2008, http://www.atmos-chem-phys-discuss.net/8/19707/2008/.

Bytnerowicz, A. and Fenn, M. E.: Nitrogen deposition in California forests: A review, Environ. Pollut., 92, 127–146, 1996.

Cahill, T. M., Seaman, V. Y., Charles, M. J., Holzinger, R., and Goldstein, A. H.: Secondary organic aerosols formed from oxidation of biogenic volatile organic compounds in the Sierra Nevada Mountains of California, J. Geophys. Res., 111, D16312, doi:10.1029/2006JD007178, 2006.

Carter, W. P. L. and Atkinson, R.: Atmospheric Chemistry of Alkanes, J. Atmos. Chem., 3, 377–405, 1985.

Carter, W. P. L.: A Detailed Mechanism for the Gas-Phase Atmospheric Reactions of Organic-Compounds, Atmos. Environ. A-Gen., 24, 481–518, 1990.

Cleary, P. A., Wooldridge, P. J., Millet, D. B., McKay, M., Goldstein, A. H., and Cohen, R. C.: Observations of total peroxy nitrates and aldehydes: measurement interpretation and inference of OH radical concentrations, Atmos. Chem. Phys., 7, 1947–1960, 2007, http://www.atmos-chem-phys.net/7/1947/2007/.

Cohen, R. C. and Goldstein, A. H.: Observations in the Foothills of the Sierra Nevada Mountains: A review motivating the Biosphere Effects on AeRosols and Photochemistry Experiment (BEARPEX), Atmos. Chem. Phys. Discuss., in preparation, 2009.

Day, D. A., Wooldridge, P. J., and Cohen, R. C.: Observations of the effects of temperature on atmospheric HNO_3, ΣANs, ΣPNs, and NO_x: evidence for a temperature-dependent HO_x source, Atmos. Chem. Phys., 8, 1867–1879, 2008, http://www.atmos-chem-phys.net/8/1867/2008/.

Day, D. A., Farmer, D. K., Goldstein, A. H., Wooldridge, P. J., Minejima, C., and Cohen, R. C.: Observations of NO_x, ΣPNs, ΣANs, and HNO_3 at a Rural Site in the California Sierra Nevada Mountains: summertime diurnal cycles, Atmos. Chem. Phys., 9, 4879–4896, 2009, http://www.atmos-chem-phys.net/9/4879/2009/.

Dillon, M., Lamanna, M., Schade, G., Goldstein, A., and Cohen, R.: Chemical evolution of the Sacramento urban plume: Transport and oxidation, J. Geophys. Res., 107, 4046, doi:10.1029/2001JD000969, 2002.

Dreyfus, G. B., Schade, G. W., and Goldstein, A. H.: Observational constraints on the contribution of isoprene oxidation to ozone production on the western slope of the Sierra Nevada, California, J. Geophys. Res., 107, 4365, doi:10.1029/2001JD001490, 2002.

Emmerson, K. M., Carslaw, N., Carslaw, D. C., Lee, J. D., McFiggans, G., Bloss, W. J., Gravestock, T., Heard, D. E., Hopkins, J., Ingham, T., Pilling, M. J., Smith, S. C., Jacob, M., and Monks, P. S.: Free radical modelling studies during the UK TORCH Campaign in Summer 2003, Atmos. Chem. Phys., 7, 167–181, 2007, http://www.atmos-chem-phys.net/7/167/2007/.

Faloona, I. C., Tan, D., Lesher, R. L., Hazen, N. L., Frame, C. L., Simpas, J. B., Harder, H., Martinez, M., Di Carlo, P., Ren, X. R., and Brune, W. H.: A laser-induced fluorescence instrument for detecting tropospheric OH and HO_2: Characteristics and calibration, J. Atmos. Chem., 47, 139–167, 2004.

Farmer, D. K., Wooldridge, P. J., and Cohen, R. C.: Application of thermal-dissociation laser induced fluorescence (TD-LIF) to measurement of HNO_3, Σalkyl nitrates, Σperoxy nitrates, and NO_2 fluxes using eddy covariance, Atmos. Chem. Phys., 6, 3471–3486, 2006, http://www.atmos-chem-phys.net/6/3471/2006/.

Farmer, D. K. and Cohen, R. C.: Observations of HNO_3, ΣAN, ΣPN and NO_2 fluxes: evidence for rapid HO_x chemistry within a pine forest canopy, Atmos. Chem. Phys., 8, 3899–3917, 2008, http://www.atmos-chem-phys.net/8/3899/2008/.

Farmer, D. K., Cohen, R. C., Perring, A. E., Wooldridge, P. J., Blake, D., Baker, A., Huey, L. G., Sjostedt, S., Tanner, D., Vargas, O., de Gouw, J., Warneke, C., Kuster, W. and Murphy, J. G.: NO_y partitioning and the role of alkyl nitrates in air quality in the Mexico City Area, Atmos. Chem. Phys. Discuss., in preparation, 2009.

Folberth, G. A., Hauglustaine, D. A., Lathière, J., and Brocheton, F.: Interactive chemistry in the Laboratoire de Météorologie Dynamique general circulation model: model description and impact analysis of biogenic hydrocarbons on tropospheric chemistry, Atmos. Chem. Phys., 6, 2273–2319, 2006, http://www.atmos-chem-phys.net/6/2273/2006/.

Fuchs, H., Brown, S. S., Dube, W., et al.: Intercomparison of instruments measuring NO_2 at the atmosphere simulation chamber SAPHIR, Atmos. Chem. Phys. Discuss., in preparation, 2009.

Gierczak, T., Burkholder, J. B., Talukdar, R. K., Mellouki, A., Barone, S. B., and Ravishankara, A. R.: Atmospheric fate of methyl vinyl ketone and methacrolein, J. Photoch. Photobio. A, 110, 1–10, 1997.

Goldan, P. D., Kuster, W. C., Williams, E., Murphy, P. C., Fehsenfeld, F. C., and Meagher, J.: Nonmethane hydrocarbon and oxy hydrocarbon measurements during the 2002 New England Air Quality Study, J. Geophys. Res., 109, D21309, doi:10.1029/2003JD004455, 2004.

Goldstein, A., Hultman, N., Fracheboud, J., Bauer, M., Panek, J., Xu, M., Qi, Y., Guenther, A. and Baugh, W.: Effects of climate variability on the carbon dioxide, water, and sensible heat fluxes above a ponderosa pine plantation in the Sierra Nevada (CA), Agr. Forest Meteorol., 101, 113–129, 2000.

Goulding, K. W. T., Bailey, N. J., Bradbury, N. J., Hargreaves, P., Howe, M., Murphy, D. V., Poulton, P. R., and Willison, T. W.: Nitrogen deposition and its contribution to nitrogen cycling and associated soil processes, New Phytol., 139, 49–58, 1998.

Grosjean, E., Grosjean, D., Woodhouse, L. F., and Yang, Y. J.: Peroxyacetyl nitrate and peroxypropionyl nitrate in Porto Alegre, Brazil, Atmos. Environ., 36, 2405–2419, 2002.

Holzinger, R., Lee, A., Paw, K. T., and Goldstein, U. A. H.: Observations of oxidation products above a forest imply biogenic emissions of very reactive compounds, Atmos. Chem. Phys., 5, 67–75, 2005, http://www.atmos-chem-phys.net/5/67/2005/.

Horowitz, L. W., Liang, J. Y., Gardner, G. M., and Jacob, D. J.: Export of reactive nitrogen from North America during summertime: Sensitivity to hydrocarbon chemistry, J. Geophys. Res., 103, 13451–13476, 1998.

Hudman, R. C., Jacob, D. J., Cooper, O. R., Evans, M. J., Heald, C. L., Park, R. J., Fehsenfeld, F., Flocke, F., Holloway, J., Hubler, G., Kita, K., Koike, M., Kondo, Y., Neuman, A., Nowak, J., Oltmans, S., Parrish, D., Roberts, J. M., and Ryerson, T.: Ozone production in transpacific Asian pollution plumes and implications for ozone air quality in California, J. Geophys. Res., 109, D23S10, doi:10.1029/2004JD004974, 2004.

Jenkin, M. E., Saunders, S. M., and Pilling, M. J.: The tropospheric degradation of volatile organic compounds: A protocol for mechanism development, Atmos. Environ., 31, 81–104, 1997.

Kirchner, F., Mayer-Figge, A., Zabel, F., and Becker, K. H.: Thermal stability of peroxynitrates, Int. J. Chem. Kinet., 31, 127–144, 1999.

Klotz, B., Graedler, F., Sorensen, S., Barnes, I., and Becker, K. H.: A kinetic study of the atmospheric photolysis of alpha-dicarbonyls, Int. J. Chem. Kinet., 33, 9–20, 2001.

Kotchenruther, R. A., Jaffe, D. A., and Jaegle, L.: Ozone photochemistry and the role of peroxyacetyl nitrate in the springtime northeastern Pacific troposphere: Results from the Photochemical Ozone Budget of the Eastern North Pacific Atmosphere (PHOBEA) campaign, J. Geophys. Res., 106, 28731–28742, 2001.

Kurpius, M. R. and Goldstein, A. H.: Gas-phase chemistry dominates O_3 loss to a forest, implying a source of aerosols and hydroxyl radicals to the atmosphere, Geophys. Res. Lett., 30, 1371, doi:10.1029/2002GL016785, 2003.

Lamanna, M. and Goldstein, A.: In situ measurements of C-2-C-10 volatile organic compounds above a Sierra Nevada ponderosa pine plantation, J. Geophys. Res., 104, 21247–21262, 1999.

Lei, W., de Foy, B., Zavala, M., Volkamer, R., and Molina, L. T.: Characterizing ozone production in the Mexico City Metropolitan Area: a case study using a chemical transport model, Atmos. Chem. Phys., 7, 1347–1366, 2007, http://www.atmos-chem-phys.net/7/1347/2007/.

Madronich, S.: Photodissociation in the Atmosphere, 1, Actinic Flux and the Effects of Ground Reflections and Clouds, J. Geophys. Res., 92, 9740–9752, 1987.

Magnani, F., Mencuccini, M., Borghetti, M., Berbigier, P., Berninger, F., Delzon, S., Grelle, A., Hari, P., Jarvis, P. G., Kolari, P., Kowalski, A. S., Lankreijer, H., Law, B. E., Lindroth, A., Loustau, D., Manca, G., Moncrieff, J. B., Rayment, M., Tedeschi, V., Valentini, R., and Grace, J.: The human footprint in the carbon cycle of temperate and boreal forests, Nature, 447, 848–850, 2007.

MCM, Master Chemical Mechansim (MCM 3.1), http://www.chem.leeds.ac.uk/Atmospheric/MCM/mcmproj.html, last access: 16 March 2009, 2003.

Mihelcic, D., Holland, F., Hofzumahaus, A., Hoppe, L., Konrad, S., Musgen, P., Patz, H. W., Schafer, H. J., Schmitz, T., Volz-Thomas, A., Bachmann, K., Schlomski, S., Platt, U., Geyer, A., Alicke, B. and Moortgat, G. K.: Peroxy radicals during BERLIOZ at Pabstthum: Measurements, radical budgets and ozone production, J. Geophys. Res., 108, 8254, doi:10.1029/2001JD001014, 2003.

Moxim, W. J., Levy, H., and Kasibhatla, P. S.: Simulated global tropospheric PAN: Its transport and impact on NO_x, J. Geophys. Res., 101, 12621–12638, 1996.

Murphy, J. G., Day, D. A., Cleary, P. A., Wooldridge, P. J., and Cohen, R. C.: Observations of the diurnal and seasonal trends in nitrogen oxides in the western Sierra Nevada, Atmos. Chem. Phys., 6, 5321–5338, 2006, http://www.atmos-chem-phys.net/6/5321/2006/.

Murphy, J. G., Day, D. A., Cleary, P. A., Wooldridge, P. J., Millet, D. B., Goldstein, A. H., and Cohen, R. C.: The weekend effect within and downwind of Sacramento - Part 1: Observations of ozone, nitrogen oxides, and VOC reactivity, Atmos. Chem. Phys., 7, 5327–5339, 2007, http://www.atmos-chem-phys.net/7/5327/2007/.

NASA, Chemical Kinetics and Photochemical Data for Use in Atmospheric Studies Evaluation Number 15, http://jpldataeval.jpl.nasa.gov/, last access: 16 March 2009, 2006.

Olszyna, K. J., Luria, M., and Meagher, J. F.: The correlation of temperature and rural ozone levels in southeastern USA, Atmos. Environ., 31, 3011–3022, 1997.

Orlando, J. J., Tyndall, G. S., and Paulson, S. E.: Mechanism of the OH-initiated oxidation of methacrolein, Geophys. Res. Lett., 26, 2191–2194, 1999.

Orlando, J. J., Tyndall, G. S., Bertman, S. B., Chen, W. C., and Burkholder, J. B.: Rate coefficient for the reaction of OH with CH_2=C(CH_3)C(O)OONO_2 (MPAN), Atmos. Environ., 36, 1895–1900, 2002.

Parrish, D. D., Dunlea, E. J., Atlas, E. L., Schauffler, S., Donnelly, S., Stroud, V., Goldstein, A. H., Millet, D. B., McKay, M., Jaffe, D. A., Price, H. U., Hess, P. G., Flocke, F., and Roberts, J. M.: Changes in the photochemical environment of the temperate North Pacific troposphere in response to increased Asian emissions, J. Geophys. Res., 109, D23S18, doi:10.1029/2004GL004978, 2004.

Perez, I. M.: The Photochemical Evolution of the Sacramento Urban Plume: a Guide to Controlling Ozone now and in a Warmer Climate, Ph.D. thesis, University of California at Berkeley, Berkeley, CA, 2008.

Perez, I. M. and Cohen, R. C.: Nitrogen oxide chemistry in an urban plume, in preparation, 2009.

Roberts, J. M. and Bertman, S. B.: The Thermal-Decomposition of peroxyacetic nitric anhydride (PAN) and peroxymethacrylic nitric anhydride (MPAN), Int. J. Chem. Kinet., 24, 297–307, 1992.

Roberts, J. M., Parrish, D. D., Norton, R. B., Bertman, S. B., Holloway, J. S., Trainer, M., Fehsenfeld, F. C., Carroll, M. A., Albercook, G. M., Wang, T., and Forbes, G.: Episodic removal of NO_y species from the marine boundary layer over the North Atlantic, J. Geophys. Res., 101, 28947–28960, 1996.

Roberts, J. M., Stroud, C. A., Jobson, B. T., Trainer, M., Hereid, D., Williams, E., Fehsenfeld, F., Brune, W., Martinez, M., and Harder, H.: Application of a sequential reaction model to PANs and aldehyde measurements in two urban areas, Geophys. Res. Lett., 28, 4583–4586, 2001.

Roberts, J. M., Flocke, F., Stroud, C. A., Hereid, D., Williams, E., Fehsenfeld, F., Brune, W., Martinez, M., and Harder, H.: Ground-based measurements of peroxycarboxylic nitric anhydrides (PANs) during the 1999 Southern Oxidants Study Nashville Intensive, J. Geophys. Res., 107, 4554, doi:10.1029/2001JD000947, 2002.

Roberts, J. M., Marchewka, M., Bertman, S. B., Goldan, P., Kuster, W., de Gouw, J., Warneke, C., Williams, E., Lerner, B., Murphy, P., Apel, E., and Fehsenfeld, F. C.: Analysis of the isoprene chemistry observed during the New England Air Quality Study (NEAQS) 2002 intensive experiment, J. Geophys. Res., 111, D23S12, doi:10.1029/2006JD007570, 2006.

Roberts, J. M., Marchewka, M., Bertman, S. B., Sommariva, R., Warneke, C., de Gouw, J., Kuster, W., Goldan, P., Williams, E., Lerner, B. M., Murphy, P., and Fehsenfeld, F. C.: Measurements of PANs during the New England air quality study 2002, J. Geophys. Res., 112, D20306, doi:10.1029/2007JD008667, 2007.

Romero, M. T. B., Blitz, M. A., Heard, D. E., Pilling, M. J., Price, B., Seakins, P. W., and Wang, L. M.: Photolysis of methylethyl, diethyl and methylvinyl ketones and their role in the atmospheric HO_x budget, Faraday Discuss., 130, 73-88, 2005.

Schade, G. W., Goldstein, A. H., and Lamanna, M. S.: Are monoterpene emissions influenced by humidity?, Geophys. Res. Lett., 26, 2187–2190, 1999.

Schade, G. W., Goldstein, A. H., Gray, D. W., and Lerdau, M. T.: Canopy and leaf level 2-methyl-3-buten-2-ol fluxes from a ponderosa pine plantation, Atmos. Environ., 34, 3535–3544, 2000.

Schade, G. W. and Goldstein, A. H.: Fluxes of oxygenated volatile organic compounds from a ponderosa pine plantation, J. Geophys. Res., 106, 3111–3123, 2001.

Sillman, S. and Samson, F. J.: Impact of Temperature on Oxidant Photochemistry in Urban, Polluted Rural and Remote Environments, J. Geophys. Res., 100, 11497–11508, 1995.

Slusher, D. L., Huey, L. G., Tanner, D. J., Flocke, F. M., and Roberts, J. M.: A thermal dissociation-chemical ionization mass spectrometry (TD-CIMS) technique for the simultaneous measurement of peroxyacyl nitrates and dinitrogen pentoxide, J. Geophys. Res., 109, D19315, doi:10.1029/2004JD004670, 2004.

Smith, D. F., Kleindienst, T. E., and McIver, C. D.: Primary product distributions from the reaction of OH with m-, p-xylene, 1,2,4- and 1,3,5-trimethylbenzene, J. Atmos. Chem., 34, 339–364, 1999.

Sparks, J. P., Roberts, J. M., and Monson, R. K.: The uptake of gaseous organic nitrogen by leaves: A significant global nitrogen transfer process, Geophys. Res. Lett., 30, 2189,

doi:10.1029/2003GL018578, 2003.

Spaulding, R. S., Schade, G. W., Goldstein, A. H., and Charles, M. J.: Characterization of secondary atmospheric photooxidation products: Evidence for biogenic and anthropogenic sources, J. Geophys. Res., 108, 4247, doi:10.1029/2002JD002478, 2003.

Staffelbach, T. A., Orlando, J. J., Tyndall, G. S., and Calvert, J. G.: The UV-visible absorption-spectrum and photolysis quantum yields of methyl glyoxal, J. Geophys. Res., 100, 14189–14198, 1995.

Talukdar, R. K., Burkholder, J. B., Schmoltner, A. M., Roberts, J. M., Wilson, R. R., and Ravishankara, A. R.: Investigation of the loss processes for peroxyacetyl nitrate in the atmosphere: UV photolysis and reaction with OH, J. Geophys. Res., 100, 14163–14173, 1995.

Tuazon, E. C., Macleod, H., Atkinson, R., and Carter, W. P. L.: Alpha-Dicarbonyl Yields from the NO_x-Air Photooxidations of a Series of Aromatic-Hydrocarbons in Air, Environ. Sci. Technol., 20, 383–387, 1986.

Tuazon, E. C. and Atkinson, R.: A product study of the gas-phase reaction of methyl vinyl ketone with the OH radical in the presence of NO_x, Int. J. Chem. Kinet., 21, 1141–1152, 1989.

Turnipseed, A. A., Huey, L. G., Nemitz, E., Stickel, R., Higgs, J., Tanner, D. J., Slusher, D. L., Sparks, J. P., Flocke, F., and Guenther, A.: Eddy covariance fluxes of peroxyacetyl nitrates (PANs) and NO_y to a coniferous forest, J. Geophys. Res., 111, D09304, doi:10.1029/2005JD006631, 2006.

Villalta, P. W. and Howard, C. J.: Direct kinetics study of the $CH_3C(O)O_2$+NO reaction using chemical ionization mass spectrometry, J. Phys. Chem., 100, 13624–13628, 1996.

Villenave, E., Lesclaux, R., Seefeld, S., and Stockwell, W. R.: Kinetics and atmospheric implications of peroxy radical cross reactions involving the $CH_3C(O)O_2$ radical, J. Geophys. Res., 103, 25273–25285, 1998.

Williams, J., Roberts, J. M., Fehsenfeld, F. C., Bertman, S. B., Buhr, M. P., Goldan, P. D., Hubler, G., Kuster, W. C., Ryerson, T. B., Trainer, M., and Young, V.: Regional ozone from biogenic hydrocarbons deduced from airborne measurements of PAN, PPN, and MPAN, Geophys. Res. Lett., 24, 1099–1102, 1997.

Williams, J., Roberts, J. M., Bertman, S. B., Stroud, C. A., Fehsenfeld, F. C., Baumann, K., Buhr, M. P., Knapp, K., Murphy, P. C., Nowick, M., and Williams, E. J.: A method for the airborne measurement of PAN, PPN, and MPAN, J. Geophys. Res., 105, 28943–28960, 2000.

Wolfe, G. M., Thornton, J. A., Yatavelli, R. L. N., McKay, M., Goldstein, A. H., LaFranchi, B., Min, K.-E., and Cohen, R. C.: Eddy covariance fluxes of acyl peroxy nitrates (PAN, PPN and MPAN) above a Ponderosa pine forest, Atmos. Chem. Phys., 9, 615–634, 2009, http://www.atmos-chem-phys.net/9/615/2009/.

Wolfe, G. M., Thornton, J. A., McNeill, V. F., Jaffe, D. A., Reidmiller, D., Chand, D., Smith, J., Swartzendruber, P., Flocke, F., and Zheng, W.: Influence of trans-Pacific pollution transport on acyl peroxy nitrate abundances and speciation at Mount Bachelor Observatory during INTEX-B, Atmos. Chem. Phys., 7, 5309–5325, 2007, http://www.atmos-chem-phys.net/7/5309/2007/.